DRI #2326

964507

REPORT

Final Report

Contract Nonr-3661 (02)

April 30, 1966

AD-633558

RESEARCH ON THE SAMARIUM-TYPE STRUCTURE OF INTRA-RARE-EARTH BINARY SYSTEMS

UNIVERSITY OF DENVER
DENVER RESEARCH INSTITUTE

UNIVERSITY OF DENVER

RESEARCH ON THE SAMARIUM-TYPE STRUCTURE OF INTRA-RARE-EARTH BINARY SYSTEMS

C. E. Lundin

University of Denver
Denver Research Institute
Denver, Colorado 80210

April 30, 1966

Technical
Final Report

Contract Nonr-3661 (02)

Department of the Navy

Office of Naval Research

PREPARED BY:

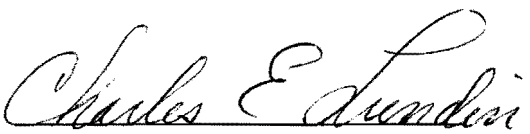

C. E. Lundin
Principal Investigator

TABLE OF CONTENTS

ABSTRACT

A total of thirteen representative intra-rare-earth binary systems were studied to determine the criteria of formation and the characteristics of the unusual samarium-type structure formed in these alloy systems. The techniques used in the studies included metallography, X-ray diffraction analysis, hardness, thermal analysis, resistivity, dilatometry, density, electron-beam microprobe analysis, and liquid-metal-solution calorimetry.

The criteria of formation of this structure was established to require a light rare earth be alloyed with a heavy rare earth. The alloy samarium-type structure was found to have the same type of microstructure, crystal structure, and similar lattice parameters compared to pure samarium metal. The compositional position of the samarium-type structure was predictable and is attributed to size factor effects. The phase equilibria were studied by many of the above techniques. It was ultimately established that a unique intermediate phase does not exist in any of the systems studied and that the room-temperature, hexagonal close-packed solid solution is continuous throughout each system. The only structural change found throughout each alloy system was one of stacking sequence. The microstructural characteristics in the binary systems were identical, suggestive that another phase was precipitating out of the terminal solid solutions. However, electron-beam microprobe traverses through "precipitate grains" showed no change in composition compared to the matrix solid solution. Furthermore, anneal-and-quench techniques, thermal analysis, resistivity, and dilatometry did not confirm the previously reported peritectoid reaction from which the intermediate phase was presumed to form. The so-called "intermediate phase" is thought to be a recrystallization phenomena, formed by the strains set up within the solid solution in the critical range of existence of the samarium-type structure. The new grains are characterized by extremely fine twinning, which is an associated mode of release of the strain, and consists structurally of the samarium-type of stacking. The mode of formation of the recrystallized grains is thought to be due to shear induced microtwinning.

The thermodynamic properties of three of the systems, the La-Gd, the Nd-Gd, and the Nd-Ho systems, were established by liquid-tin-solution calorimetry. The heats of solution of the components; La, Nd, Gd, and Ho in indium were first determined. The heats of

solution of the alloys were then determined. From these data the heats of mixing in the alloy systems were then calculated. These data are presented in both tabular and graphical form. There were no inflections or significant changes in slope of the heats of mixing versus composition curves at the compositions where the samarium-type structures exist, confirming that first-order phase transformations do not exist.

I. INTRODUCTION

This final technical report describes the investigations conducted for the Office of Naval Research on a program entitled "Research on the Samarium-Type Intermediate Phases of Intra-Rare-Earth Binary Systems." The report is submitted in compliance with the terms of Contract No. Nonr-3661 (02) between the Office of Naval Research, Department of the Navy, and the Denver Research Institute, University of Denver. The period covered by this report is from (1 January 1962 to 30 April 1966.) 9

The purpose of this program was to determine the criteria necessary to the formation of the samarium-type structure observed in intra-rare-earth binary alloy systems. The nature and characteristics of these systems and the samarium-type structure were to be determined, and a correlation of the structural and compositional dependence and mode of formation of the samarium structure with atomic size, electronic structure, crystal structure, and other variables in the pure components would be attempted. The scope of the research was intended to provide a sound basis for a better understanding of the alloying behavior of intra-rare-earth alloy systems.

Because of their marked similarities, yet subtle differences, the rare earths form a unique and metallurgically interesting group of elements. It was recognized that these properties could lead to a systematic study, yielding much fundamental knowledge concerning the principles of metal and alloy behavior. It is both interesting and significant that many properties of the rare earths can be approximately expressed as linear functions of the atomic number. This is attributed to the consecutive filling of the inner 4F shell with electrons, which contributes to a tighter binding of the atom as atomic number is increased. The result can be directly observed in the almost linear lanthanide contraction.

The majority of the rare earths crystallize at room temperature in the hexagonal-close-packed system, while cerium, europium, and ytterbium exhibit a face-centered, body-centered, and face-centered cubic room temperature structure, respectively. The rare earths can be separated into two groups according to their subtle differences in properties, the light rare earths and the heavy rare earths. These two groupings are important because they bear in an important manner on the findings in this report. Among the light rare

earths (La to Nd), the predominating hexagonal-close-packed structure is the Lanthanum (A3') type, with the packing sequence, ABAC. The heavy rare earths (Gd to Lu) are of the Magnesium (A3) type. Yttrium and scandium also have the A3 type structure. Samarium on the other hand, crystallizes in a hexagonal-close-packed structure with a multiple-packing sequence, ABABCBCAC.

The rare-earth metals traditionally have been considered so identical in character that very little research on intra-alloying effects has been conducted. Ten years ago physical metallurgists and solid-state physicists considered alloy studies between rare earth metals as too academic. Recently, the dearth of studies has been rectified, in that, more work is finally reaching the literature, and such research is unveiling some extremely interesting phenomena, as is the case in this study. The peculiar behavior of intra-rare-earth binary alloy systems was first observed by this author in a phase diagram study of the Ce-Y system conducted by Lundin and Klodt[1] in 1958, but was not recognized at that time for its proper significance. At the same time, Spedding, Valletta, and Daane[2] conducted a similar study on the La-Y and La-Gd systems. In both cases, the authors reported the existence of an "intermediate phase" in each of these systems, having the samarium structure. Other binary studies had been reported in the literature at that time, but the components consisted of either two light-rare-earths or two heavy-rare-earth components. These combinations exhibited completed solid solubility with no significant microstructural anomalies. The difference in the phase equilibria in these two types of systems had a suggested explanation. The systems reported to have an intermediate phase were combinations of light rare earths with heavy rare earths, while those with complete solid solubility were not. The curious nature of the formation of this unusual structure in such systems was the impetus which led to this study. Thus, it was hoped to determine whether the hypothesized criteria of formation of this structure was borne out in the study of other combinations of binary systems and, if so, what the mode of formation and character of such a structure was. It also seemed apparent that in the periodic series of rare earth metals, samarium was a transition between the light and heavy rare earths. This is exemplified by the crystal structure and other properties. Thus, if one obtains a transition phase on alloying a light and heavy rare earth, isomorphous in structure with samarium metal, there is probably a basis for a correlation between why it exists in these alloys and likewise in the elemental series of lanthanons. Size effect appeared to be a logical

premise. It was deemed conceivable that a critical size factor exists in the alloy solid solutions wherein the most stable packing would be that of the samarium structure. It follows that the relative compositional position of this structure in the binary system would be related to size effect. Since the interatomic distances of the lanthanons as a function of increasing atomic number are linear, the position of the transition structure would be approximated by a weighted average of the two components. The "synthesis" of the samarium metal structure by alloying has proven to be the most challenging and interesting concept to be developed during the course of the program. The confirmation of these preliminary speculations on initiating the program were the major objectives sought. Most of these speculations have been proven to be valid as will be described in the text which follows. The one major exception is that the intermediate phase does not exist and that the phase observed is a strain induced recrystallization phenomenon which has the samarium-type structure.

II. EXPERIMENTAL PROCEDURE

A. Materials

The highest purity rare-earth metals available were purchased for this study from various sources. The metals, their sources, and nominal purities are listed below:

Lanthanum	Lunex Co.	99.9 %
Cerium	Bureau of Mines (Reno)*	99.9 %
Neodymium	Lunex Co.	99.9+%
Samarium	Ames Laboratory	99.9 %
Gadolinium	Lunex Co.	99.9+%
Holmium	Lunex Co.	99.9+%
Lutetium	United Mineral and Chemical Corp.	99.9 %
Yttrium	Ames Laboratory	99.4 %
Scandium	Johnson, Matthey and Co., Ltd	99+ %

The detailed impurity elements and their concentrations are listed in Table I.

The indium* used for the liquid-metal-solution calorimetry was obtained from the Indium Corporation of America and is reported to be 99.99%.

B. Alloy Preparation

The as-received rare-earth metals were sectioned by hacksaw and cut with a jeweler's saw into small pieces suitable for weighing. These pieces were then filed with a clean file to obtain surfaces free from contamination. Clean tweezers were employed for all further handling after this stage of preparation. The charges for melting were prepared by weighing on an analytical balance to the nearest 0.1 mg. Lanthanum and cerium charges, because of their reactivity, were cut

* The cerium and the indium metals were donated by their respective sources.

TABLE I

Analyses of Rare-Earth Metals

Element	Lanthanum	Cerium	Neodymium	Samarium	Gadolinium	Yttrium	Holmium	Lutetium	Scandium
O_2	510 ppm	60 ppm	140 ppm	---	210 ppm	1850 ppm	125 ppm	*	*
N_2	2	---	6	< 25 ppm	---	120	---		
C	---	500	---	30	---	80	---		
Other Rare earths	330	---	50	≤400	325	330	110		
Si	50	30	---	---	---	20	---		
Fe	---	220	---	20	---	60	---		
Mn	---	---	---	---	---	6	---		
Mg	50	---	---	---	50	10	---		
Al	1	140	---	---	1	10	---		
Ta	10	---	---	---	10	60	---		
Ni	1	---	1	---	1	60	---		
Cu	1	50	1	---	1	20	1		
Ca	10	---	10	500	---	10	10		
Cr	1	---	1	---	1	20	1		
V	---	---	1	---	---	---	1		
B	---	---	50	---	---	3	---		
Nb	---	---	---	---	---	---	---		
Na	---	---	---	---	5	---	---		
Be	10	---	10	---	10	1	---		
K	1	---	---	---	1	6	---		
Ti	1	---	---	---	1	---	---		
Co	1	---	1	---	1	<100	---		
Zn	50	---	50	---	50	<100	50		
Zr	20	---	20	---	20	3000	---		
Cd	---	---	5	---	---	3	---		
Ce	50	99.87%	---	---	50	---	---		
Mo	---	200	---	---	---	---	---		
W	---	40	---	---	---	---	---		

* No detailed analysis available

and filed under an inert atmosphere in a dry box. Weighing was conducted rapidly, and the charges were placed immediately in the melting furnace which was subsequently evacuated. Exposure to air after cleaning and weighing was, therefore, kept to a minimum to prevent oxidation.

The melting was conducted under a slightly positive pressure of purified argon in a non-consumable electrode arc furnace. To ensure homogeneity the buttons of about 20g were inverted and remelted four times at 200 amp. The arc furnace and accessories are standard equipment, and the procedures have been described in the literature.

Weighing of the buttons after melting indicated negligible weight losses due to vaporization. Melting losses were consistently less than 0.05 w/o.

During the melting phase, weight losses were negligible. No chemical analyses were deemed necessary. The nominal compositions of the buttons were selected on the basis of atomic percent. These buttons were then stored in a vacuum dessicator until required for further study.

Difficulty was had in melting alloys in the lutetium alloy systems, particularly in the La-Lu system. It is suspected that the wide variation in melting points and/or density had a bearing on the melting characteristics. Some of the buttons were characterized by gross inhomogeneities to such a degree that macrostructures of button cross-sections clearly indicated the lutetium was only partially melted. Apparently the lutetium was sufficiently more dense than the lanthanum that it settled rapidly to the bottom of the liquid lanthanum. These buttons were arc melted with more than enough power to melt even pure lutetium. However, the lutetium cooled sufficiently near the bottom of the melt to prevent its melting and dissolution. The standard procedure has been to invert the alloy buttons and remelt about 4 to 6 times. The other rare earth binary alloys were melted with ease by this technique. To assure complete dissolution, the Nd-Lu alloys were inverted and remelted a total of 12 times. This procedure eliminated most of the inhomogeneity in this system, but not in the La-Lu system where the density and melting point differences are still greater between components. Some of the La-Lu alloys were melted 28 times and still showed signs of inhomogeneity. By this time many of the buttons had become contaminated with copper from the arc-furnace hearth and oxygen from handling.

C. Heat Treatment

Metallographic examinations of the as-cast buttons revealed coring in the microstructures. It was therefore deemed desirable to give these alloys a homogenization treatment to restore equilibrium conditions. The alloy buttons were first wrapped in tantalum foil and then sealed in Vycor capsules under a partial pressure of argon. This tantalum foil served the dual purpose of providing protection to the specimen and physical support to the walls of the Vycor capsules. The capsules containing the samples were annealed in a resistance-wound, vertical tube furnace. Furnace temperatures were maintained for several hours at the desired level before the capsules were placed in the furnace. The temperature control was ± 2°C of the desired temperature. At the conclusion of the anneals the specimens were cooled rapidly to retain the high-temperature structures.

The homogenization temperatures and times are presented below for the thirteen systems studied.

System	Homogenization Temperature, °C	Time, Hr.
La-Gd	800	150
La-Y	650	150
La-Ho	650	32
La-Lu	800	16
La-Sc	800	16
Ce-Gd	650	32
Ce-Y	650	150
Ce-Ho	650	32
Nd-Gd	800	16
Nd-Y	650	150
Nd-Ho	800	16
Nd-Lu	800	16
Sc-Gd	800	16

D. Metallography

The preparation of suitable surfaces of rare-earth metals or alloys for metallographic study is at best difficult. Two principal problems contribute to this difficulty. First of these is the attainment of a surface free of reaction products either from the etchant or air

oxidation, and the second is a surface free from disturbed metal. Two metallographic techniques were developed, which are described below.

The metallographic specimens were first cut from the arc-cast button with a jeweler's saw to minimize heating and working of the alloy. This specimen was mounted in a cold-setting dental plastic not requiring heat and pressure for forming as does bakelite. Grinding was slowly carried out by hand with a solution of paraffin and Deobase (purified kerosene) as a lubricant and coolant. The grinding was done in stages with successive reductions in grit size, using 120, 240, 400, and 600 mesh papers in that order. A Syntron Vibratory Polisher, which polishes with a minimum of applied pressure, was employed for the polishing operation. The polishing was carried out in two stages. In the first stage, a slurry of Deobase and 5-micron alumina (Buehler AB #1) was used as a polishing medium with the Syntron operating at moderate amplitudes for $2\frac{1}{2}$ to 3 hours. The second stage of polishing was performed with a slurry of 0.3-micron alumina and Deobase. Synasol (denatured alcohol) was employed for rinsing between grinding and polishing stages, as water would react with the surface of the specimens.

A mixture of approximately three parts glycerol to one part of concentrated nitric acid was found suitable as a general etchant for all the rare-earth metals and alloys, with the exception of lanthanum-rich alloys. These require a milder etchant consisting of four to five parts of glycerol to one part of concentrated nitric acid. The etchant was applied by swabbing vigorously for 3 to 5 seconds with a saturated cotton swab. Immediate rinsing with profuse amounts of Synasol was employed to stop the etching action. The etchant is prepared fresh before each using, because it deteriorates in a few hours.

It was felt that this technique could be improved on, so considerable effort was expended to attempt another approach, namely, electrolytic polishing and etching. These efforts were successful since a reliable, reproducible electrolytic method was developed. The procedure is as follows. The rough grinding was conducted similar to that in the previous procedure. The polishing and etching stages were carried on completely by electrolytic techniques. A stainless-steel cathode was employed, and the metallographic specimen, which was mounted in plastic, acted as the anode. Contact was made with the rare-earth metal or alloy by a special tweezer-clamp arrangement.

The specimen was immersed by hand in the electrolyte while electrical continuity was maintained by one prong of the tweezers in contact with the specimen. An ice bath was necessary to cool the electrolyte solution. The electrolyte consisted of various mixtures of methanol and nitric acid. The voltage setting of the power source, the times of immersion, and the composition of the electrolyte were adjusted for each alloy system. The area of specimen exposed was of the order of 25 sq mm. The nominal voltages varied from 3 to 6v, the time of immersion from 5 to 30 sec, and the solution from 2 to 4 parts methanol to 1 of HNO_3.

E. Thermal Analysis

Thermal analyses were conducted on several pure metals to determine the characteristics of known phase transformations. Pure iron and neodymium metal were employed, and the equipment calibrated. The alloy specimens which were presumed to be the intermediate phase compositions were then analyzed in an attempt to locate the temperature of transformation to the samarium-type structure.

All measurements were made in a high-vacuum system at less than 10^{-6} torr. The heating source was provided by a tungsten spiral coil, thermally heat shielded by three concentric tantalum shields. The specimen consisted of a machined cylinder of the metal to be studied, 3/4 in. long by 1/2 in. in diam. A 1/8 in. diam. hole was drilled in one end to the center of the cylinder. A chromel-alumel thermocouple was inserted, insulated with recrystallized alumina. The tip of the thermocouple was welded to the metal to obtain direct contact. The specimen was heated and cooled through the expected temperature range of transition at a rate of about 10°C per min. The temperature was measured to ± 2°C. At least three runs were made per specimen. The time versus temperature data were then plotted and analyzed for arrests or inflections.

F. Resistivity Measurements

In conjunction with the thermal-analysis measurements, resistivity versus temperature determinations were conducted to locate the proposed phase transformation temperatures to the samarium-type intermediate phase. Since the thermal analysis did not demonstrate evidence of reproducible and uncontrovertible inflections or arrests, it was thought that resistivity would be more sensitive. A

resistivity apparatus and a vacuum furnace were assembled for this purpose. The vacuum furnace was the same unit employed for the thermal-analysis studies, except that the specimen assembly inside of the heat shields was different. The specimen consisted of a cylinder of the metal to be studied, 1/8 in. in diam. by 3/4 in. long. Tantalum wire of about .020 in. in diam. was used for the potential and current leads. These leads were spot welded by an arc-discharge technique to the specimen in an argon atmosphere. A test length of 1/2 in. was used. These leads and a chromel-alumel thermocouple were introduced by means of an O-ring-sealed base plate through an Amphenol connector. The vacuum maintained during the experiments was 10^{-6} torr or less. The temperature was raised and lowered through the designated temperature range at least three times per specimen at a rate of about 10°C per min. A Kelvin double-bridge of one μ-ohm sensitivity was employed to determine the resistance of the specimen. In conjunction with the Kelvin double-bridge, a Leeds and Northrup galvanometer, a Rubicon low-resistance standard slide wire, and a Rubicon Precision potentiometer were used in the measuring circuit. The temperature was measured to within ± 2°C. The time versus resistivity data were plotted and analyzed to detect the thermal arrests.

G. X-Ray Diffraction Analysis

The powder method of X-ray diffraction was the principal technique employed on all phases of the X-ray investigation. Samples were reduced to powder by filing, and the powders were passed through a 325-mesh screen. The screened powders were then packed into quartz capillary tubes having a uniform wall thickness of 0.01 mm and an inside diameter of 0.50 mm. It was necessary to perform all of the above procedures in an atmosphere of argon to eliminate oxide contamination of the powders. The capillaries were then mounted on a vacuum manifold, purged, evacuated and sealed with an oxy-hydrogen torch. The powder specimens were then annealed for 2 hrs. at 300°C to relieve the cold work produced during filing. Specimens prepared in this manner evidenced no oxide contamination during subsequent X-ray diffraction studies.

A 114.6-mm diameter Debye-Scherrer camera was employed to determine the characteristic line patterns of the samples. The annealed powders were removed from the capillaries and were mounted on the surface of a 0.2 mil fiberglass filament with vaseline. Patterns were obtained with CuK_α radiation using 30 kv and 30 ma. The exposure time was normally about 12 hr.

The data obtained from the Debye-Scherrer camera were employed for phase identification and also for calculation of precise lattice parameters and X-ray densities. The unsymmetrical, or Straumanis, method of film loading was employed to provide correction factors for film shrinkage and unprecise camera dimension. Line positions were measured to an accuracy of 0.05 mm on a vernier scale illuminator. The film data were reduced on the Burrows 205 computer. Input data consisted of 2S (theta in millimeters), which was read directly from the film, and the film shrinkage and camera radius correction factor. The computer internally calculated d-spacings, "Q" values, $\sin^2\theta$ and $\sin^2 2\theta$. The Q ($Q = 1/d$), $\sin^2\theta$ and $\sin^2 2\theta$ values were used to facilitate phase identification and line indexing. Subsequent to phase identification precise lattice parameters for each phase present were determined.

The computer program, corrected for absorption, conducted trial indexing until the best fit was produced, obtained the lattice parameters by use of Cohn's least squares technique, and these parameters in turn were used to obtain new indices.

The Laue back-reflection technique was used during the course of the program to analyze single grains of pure samarium and several of the alloys. The objective was to determine whether twinning occurred. The twinned structures would be confirmed by the production of pairs of back-reflected diffraction spots. Copper radiation, filtered with nickel, was employed with the alloys. Two-hour exposures were made at 30 ma and 30 v. Chromium radiation filtered with vanadium was employed on pure samarium with six-hour exposures.

H. Liquid-Metal-Solution Calorimetry

The liquid-metal-solution calorimeter was an isothermal calorimeter which was designed to operate to 500° C. Normally, tin has been used as the solvent because of its purity, low melting point, low vapor pressure, and its well-established heat capacity. However, tin proved to be unsatisfactory in the rate of dissolution of the heavy-rare-earth metals. The light rare earths dissolved in tin, but rather slowly. Bismuth was then tried and again no success was had with bismuth. A further complication with bismuth was its high vapor pressure. Indium metal was tried next with the rare earths; lanthanum, neodymium, gadolinium and holmium. The lanthanum, neodymium and

gadolinium dissolved rapidly, but the holmium was somewhat slower. However, good data were still obtainable with these rates of solution, whereas it would have been impossible with the tin. Furthermore, indium has all of the attributes that tin has for a suitable liquid medium.

The indium was contained in pyrex tubes in the amount of about 35g and was stirred constantly at 10 rpm by a molybdenum stirring mechanism. The pyrex tube was contained in an evacuated calorimeter well. Samples were added by gravity without breaking vacuum. Two calorimeter wells were employed during an experimental run, one well was the sample drop well, and the other was the standard well. The wells were located in and insulated from a massive aluminum block which was maintained at a constant temperature. To monitor the heat effect of a sample drop, the difference in temperature between the two wells was determined by two multijunction thermopiles. Forty-eight junctions were distributed over the surface of each well. A matching set was placed next to the aluminum calorimeter block in which the wells are located. The electrical output was thus the true temperature difference between the two reaction wells. The output of the differential thermopile was introduced to a DC amplifier. In turn, the output of the amplifier was fed into a Leeds and Northrup strip-chart recorder.

The aluminum calorimeter block was contained in a cylindrical furnace, with both cylindrical- and end-type heaters. The control heater was controlled by a resistance thermometer and powered by a saturable-core reactor operating from a resistance bridge. Excellent temperature control, with maximum cycling of about 1/3°C, was had. Surrounding this assembly was an evacuated chamber and another final outer chamber containing Silocel insulating powder.

A typical heat perturbation from an unknown sample gave rise to an EMF output on the differential thermopile which increased or decreased depending on whether the heat was exothermic or endothermic. It reached a peak and then decayed exponentially back to the original base value, indicating that the temperatures of the two wells were again identical. The strip chart recorded the time-temperature curve. Initially, the calorimeter was calibrated by dropping a known material in the bath such as solid indium. The heat-transfer coefficient was calculated from the rate of decay of the time-temperature curve. The calorimeter heat capacity was determined, knowing the total heat evolved from the solution of a known standard.

The heat effect of the dissolution reaction of an unknown was calculated according to a method described by Howlett, Leach, Ticknor, and Bever.[3] All samples were added to the liquid metal bath from OC. They were maintained under vacuum in an ice bath and allowed to equilibrate prior to the addition. The calculated heat effect for each sample was divided by the number of moles of material giving the relative partial molal heat of solution in indium. From these data the heats of solution were calculated.

III. RESULTS AND DISCUSSION

A. Scope of Study

The study of intra-rare-earth binary systems and the reported intermediate phase was initiated to thoroughly amplify the meager information available concerning unusual behavior of these systems. On the basis of the first three systems studied, the Ce-Y system by Lundin and Klodt[1] and the La-Y and La-Gd systems by Spedding, Valletta, and Daane,[2] certain hypotheses were made in the initial phase of study which required confirmation. The confirmation could only be realized by selecting a representative cross-section of intra-rare-earth binary systems and conducting a thorough, multiphased study. The hypotheses originally proposed were as follows:

1. The criterion of formation of the samarium-type intermediate phase is that it can only be formed by alloying a light rare earth with a heavy rare earth.

2. The compositional position of the phase is analytically predictable.

3. The compositional position of the intermediate phase is size-factor dependent.

All of these hypotheses can now be substantiated, with one exception. The intermediate phase does not exist as a first-order transformation product; instead, the samarium-type structure occurs by means of a recrystallization phenomenon, probably due to a strain mechanism. (It will henceforth be termed the samarium-type structure or phase rather than be called an intermediate phase.) The crystal structure is unique compared to those of the terminal solid solutions, but retains a fixed composition during cooling throughout the range of temperatures wherein the hexagonal close-packed modification is stable. The first proposed phase diagrams, which explained the presence of the unique samarium-type structure by means of a peritectoid reaction at some intermediate, must now be modified accordingly. These considerations will be justified and amplified in subsequent sections.

Thirteen representative systems were selected from all of the possible combinations of light-and heavy-rare-earth metals. The systems chosen are presented below.

La-Gd	Ce-Ho
La-Y	Nd-Gd
La-Ho	Nd-Y
La-Lu	Nd-Ho
La-Sc	Nd-Lu
Ce-Gd	Gd-Sc
Ce-Y	

The considerations employed in selecting these systems to provide the most representative cross-section were systematic. Table II presents the crystallographic data for the rare earth metals, scandium, and yttrium for a comparison of their structural characteristics. The extreme members of the light-rare-earth series, whose ambient structures are hexagonal close-packed, La type (ABAC packing), are lanthanum and neodymium in order of increasing atomic number. The extreme members of the heavy-rare-earth series, whose ambient structures are hexagonal close-packed, Mg A3 type (ABAB packing), are gadolinium and lutetium. Samarium was considered to be a transition between the light and heavy rare earths. Europium and ytterbium are excluded from this study, since they have entirely different room-temperature structures, body-centered cubic and face-centered cubic, respectively. Furthermore, they react more like alkaline earth elements in all of their other properties. In order to encompass all intermediate systems, various combinations of these extreme members of the light and heavy rare earths were selected for study as follows. The lightest light rare earth was alloyed with the lightest heavy rare earth, namely La-Gd. The heaviest light rare earth was alloyed with the heaviest heavy-rare earth, namely Nd-Lu. The lightest light rare earth was alloyed with the heaviest heavy-rare earth, namely La-Lu. The heaviest light rare earth was alloyed with the lightest heavy rare earth, namely Nd-Gd. All other alloy systems would be intermediate to these. However, since the heavy rare earth series is rather long, holmium was chosen in the middle of this series to alloy with lanthanum and neodymium, respectively. Several other members of the series were of interest for other reasons. Since cerium is rather unique and more complex in its crystal chemistry than the other light rare earths,

TABLE II

Crystallographic Data for Rare-Earth-Metals[4]

Element	Temp. Range, °C	Structure	Lattice Constants, Å	c/a ratio†	Density, g/cm³	Atomic Vol., cm/mole³	Metallic*** Radius, A
Sc	room to 1000	h.c.p.	a = 3.3080 c = 5.2653	1.5917	2.992	15.028	1.655
Y	room to 1495	h.c.p.	a = 3.6451 c = 5.7305	1.5722	4.478	19.86	1.778
	1495 to mp	b.c.c.	a = 4.11‡	---	---	---	
La	-271 to 310	hex.	a = 3.770 c = 12.131	1.610	6.174	22.50	1.885
	310 to 868	f.c.c.	a = 5.303	---	6.186	22.46	
	868 to mp	b.c.c.	a = 4.26	---	5.98	23.2	
Ce	below - 150	f.c.c.	a = 4.85	---	8.23	---	1.825
	-150 to -10	hex.	a = 3.68 c = 11.92	1.62	---	---	
	-10 to 730	f.c.c.	a = 5.1604	---	6.771	20.695	
	730 to mp	b.c.c.	a = 4.12	---	6.67	21.0	
Pr	up to 798	hex.	a = 3.6702 c = 11.828	1.61	6.782	20.778	1.836
	798 to mp	b.c.c.	a = 4.13	---	6.64	21.2	
Nd	up to 868	hex.	a = 3.6582 c = 11.802	1.612	7.004	20.60	1.829
	868 to mp	b.c.c.	a = 4.13	---	6.80	21.2	
Sm	up to 917	rhomb.	a = 8.996 α = 23°13'	1.61	7.536	---	1.811
	917 to mp	---	---	---	---	---	
Eu	to mp	b.c.c.	a = 4.578	---	5.259	28.91	1.994
Gd	to 1262	h.c.p.	a = 3.6315 c = 5.777	1.591	7.895	19.88	1.810
	1262 to mp	b.c.c. (?)	a = 4.06	---	7.8	20.2	
Tb	to 1310	h.c.p.	a = 3.5990 c = 5.696	1.583	8.272	19.245	1.800
	1310 to mp	?	---	---	---	---	
Dy	to 950**	h.c.p.	a = 3.5923 c = 5.6545	1.574	8.536	19.032	1.795
Ho	to 966**	h.c.p.	a = 3.5761 c = 5.6174	1.571	8.803	18.742	1.789
Er	to 917	h.c.p.	a = 3.5590 c = 5.592	1.571	9.051	18.473	1.779
Tm	to 1004	h.c.p.	a = 3.5372 c = 5.5619	1.572	9.332	18.151	1.769
Yb	to 798	f.c.c.	a = 5.481	---	6.977	24.80	1.940
	798 to mp	b.c.c.	a = 4.44	---	6.54	26.5	
Lu	to 1400	h.c.p.	a = 3.5050 c = 5.5486	1.583	9.842	17.779	1.752

*h.c.p. = hexagonal close-packed
hex. = hexagonal, with c/a = 3.2
f.c.c. = face-centered cubic
b.c.c. = body-centered cubic
rhomb = rhombohedral

†Normalized to twice the distance between close-packed planes.

‡ Value calculated by Gschneidner

** Possible transition at higher temperatures.

*** Reference 5

several alloy systems were chosen with cerium as one component, namely Ce-Gd, Ce-Y, and Ce-Ho. Yttrium is thought of as a heavy rare earth since it is isomorphous in structure and always associates in nature with the rare earths due to similar chemical properties. Therefore, yttrium was included to determine whether it also conformed to the general hypotheses of intermediate phase formation. The systems chosen with yttrium as one component were La-Y, Ce-Y, and Nd-Y, which represent the whole range of light-rare-earth additions. Finally, scandium, a member of the Group III B Transition metals which should be very similar to yttrium, lanthanum, and the other lanthanons, were selected to determine whether it was close enough in structural characteristics to form the intermediate phase. Scandium has a small metallic radius (1.641A) compared to yttrium (1.801A) and the other rare earth metals (1.877-1.734A). Thus, it was presumed to act more like a heavy rare earth than a light rare earth strictly from size considerations. Thus, the systems, La-Sc and Gd-Sc, were analyzed to determine whether the samarium-type structure would form with either the light-rare-earth addition, lanthanum, or the heavy-rare-earth addition, gadolinium. In neither case did the samarium-type structure appear in these systems. Thus, as one would suspect, scandium acts more like the neighboring transition metals, titanium and zirconium, than it does the rare earth metals. The overall scope of binary systems in this program was considered sufficiently representative and broad in coverage that any other combination can be assured to form the samarium-type structure.

The alloys prepared for each system are presented in Table III. A total of 150 alloys were arc melted and studied by the various techniques during the course of the program. The pure elements of each component in the binary systems were also arc melted.

On the basis of the principles of alloying theory, the properties of the component rare earth metals are similar enough to expect extensive, if not complete, room-temperature solid solubility in any combination of binary systems. The electronegativities[6] are essentially the same, varying from 1.17 for lanthanum to 1.22 for lutetium. This dictates against the formation of intermediate phases. The valences are consistently three throughout the series of rare earths. The crystal structures are all basically hexagonal-close-packed with only subtle differences in the stacking sequence between the light and heavy rare earths. The largest size factor difference of any combination of binary systems in the lanthanon series is for the La-Lu system, or 7.6 percent. The La-Sc has the

TABLE III

Intra-Rare-Earth Binary Alloys

La-Gd a/o La	La-Y a/o La	La-Ho a/o La	La-Lu a/o La	La-Sc a/o La	Ce-Gd a/o Ce	Ce-Y a/o Ce
10	20	30	20	85	5	30
12	36	35	30	70	10	35
14	38	40	40	55	15	40
16	40	42.5	50	40	20	45
18	42	45	60	25	25	50
20	44	47.5	64	10	27.5	55
22	46	50	70		30	60
24	48	55	80		32.5	65
26	50	60			35	70
28	52	65			37.5	75
30	54	70			40	
32	56				45	
34	58					
36	60					
38	70					
40	80					
42						
44						
46						
50						
60						

Ce-Ho a/o Ce	Nd-Gd a/o Nd	Nd-Y a/o Nd	Nd-Ho a/o Nd	Nd-Lu a/o Nd	Gd-Sc a/o Gd
35	20	40	50	20	85
40	30	45	55	40	70
45	35	50	60	50	55
50	40	55	65	60	40
55	45	60	70	70	25
60	50	65	71	80	10
65	55	69	75	82	
70	60	70	80	90	
75	65	75	85		
	70	80	90		
	80	85			
		90			
		95			

greatest difference of all the rare-earth-like elements considered, or 13.9 percent. Scandium is a special case, since it is considered a borderline rare earth compared to yttrium and the lanthanon series (it has a considerably smaller metallic radius). The La-Sc system was found to exhibit two-phase immiscibility in this study, which is not surprising. It is interesting, however, that it did not form the samarium-type structure, because it had all of the qualifications and properties of any of the other light-heavy binary combinations, except that the size factor was not favorable. It must be pointed out that electronic structure differences cannot be attributed to the immiscibility observed. The La-Y system, also having a gross electronic structure difference, exhibited no immiscibility, but showed the presence of the samarium-type structure. Its size factor is favorable. This emphasizes the importance of size factor in the formation of the samarium structure. The Gd-Sc system has a size factor difference of 9.4 percent, yet it was found to exhibit complete solid solubility. This combination has the highest size factor difference of all of the combinations among those components which have the Mg A3 type packing. However, it does not comply with the criteria of formation of the samarium-type structure, namely a light and heavy rare earth by alloyed. The remaining systems studied were all observed to have the samarium-type structure and the same microstructural features, with two exceptions. There is no doubt that any other combinations would be isostructural and isomorphous. The two exceptions were the La-Lu and Nd-Lu systems. They exhibited a two-phase immiscibility gap in the low-temperature region. The Nd-Tm system was reported to have a samarium-type structure,[2] and its size-factor difference is less than the La-Lu system. The only reason that can be advanced to explain this exception to the general criteria is that lutetium does not act like a rare earth in this respect, but more like the adjacent transition metals.

The techniques selected to analyse the systems for their structural characteristics were metallography, X-ray diffraction analysis, hardness, thermal analysis, resistivity, dilatometry, density, electron-beam microprobe analysis, electron transmission analysis, and liquid-metal-solution calorimetry. The most useful and revealing of the techniques in studying the characteristics of the systems were metallography, X-ray diffraction analysis, electron-beam microprobe analysis, and liquid-metal-solution calorimetry. The remaining techniques were auxiliary and only lent further credence to the information obtained by the four principal methods.

The thermodynamics of three of the systems, the La-Gd, the Nd-Gd, and the Nd-Ho systems, were determined in the last major phase of the program by liquid-metal-solution calorimetry. These data were not only used to delineate the structural features of the systems, but, even more noteworthy, to establish the heats of solution of the metals and the various alloys in liquid indium and, in turn, to calculate the heats of mixing as a function of compositions in the three systems.

B. Metallographic Analysis

In the initiation of these studies, the determination of the phase equilibria of the various systems was felt to be the principal objective, since at that time, several phase diagram studies[1, 2] had reported the anomalous existence of an intermediate phase. How the compositional dependence of the intermediate phase varied as a function of the binary components was not yet clear. The intermediate phase and the associated phase equilibria were first reported in the investigations of the Ce-Y system by Lundin and Klodt[1] and the La-Gd and La-Y systems by Spedding, Vallette, and Daane[2]. The phase diagrams are presented in Figures 1, 2, and 3. Since then, several additional studies have been reported, wherein the phase equilibria were essentially proposed to be the same. The Nd-Y system was cursorily outlined by Kirkpatrick and Love[7] in which the existence of an intermediate phase was reported. Burov, Terechova, and Savitsky[8] investigated the Ce-Gd system, and Beaudry, Michel, Daane, and Spedding[9] established the Y-Nd system. In both of these latter phase diagram studies, the reported equilibria were isomorphous with the earlier work. The intermediate phase in all cases was reported to have the samarium structure by X-ray diffraction analysis. Other intra-rare-earth binary alloys have been investigated by X-ray diffraction analysis only and have been reported to have the samarium-type structure, as follows; Nd-Y, Nd-Tm, Pr-Y.

Metallographic examination of both as-received and as-melted ingots showed evidence of oxide second phase, which is clearly discernible. However, since the oxide phase remains essentially inert to the metallic equilibria, very little effect on the phase equilibria is expected. Singling out this impurity phase in the component metals and all of the alloys was not difficult, so it did not provide any problems such as masking the phase equilibria. The structures of the eight rare-earth metals; lanthanum, cerium, neodymium, gadolinium, holmium, lutetium, yttrium, and scandium, are presented at a magnification of 250X in Figures 4 through 11, respectively. The lanthanum,

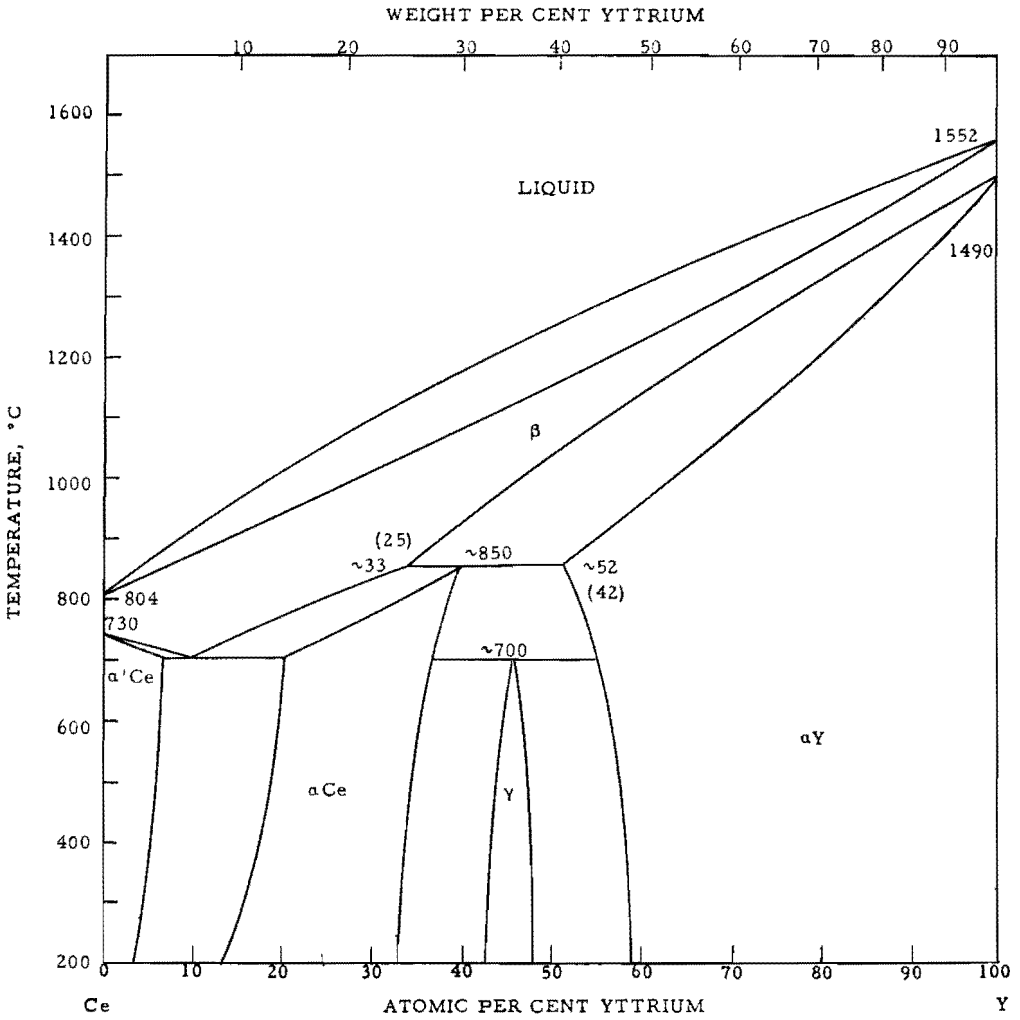

Figure 1. The Equilibrium Phase Diagram, Cerium-Yttrium

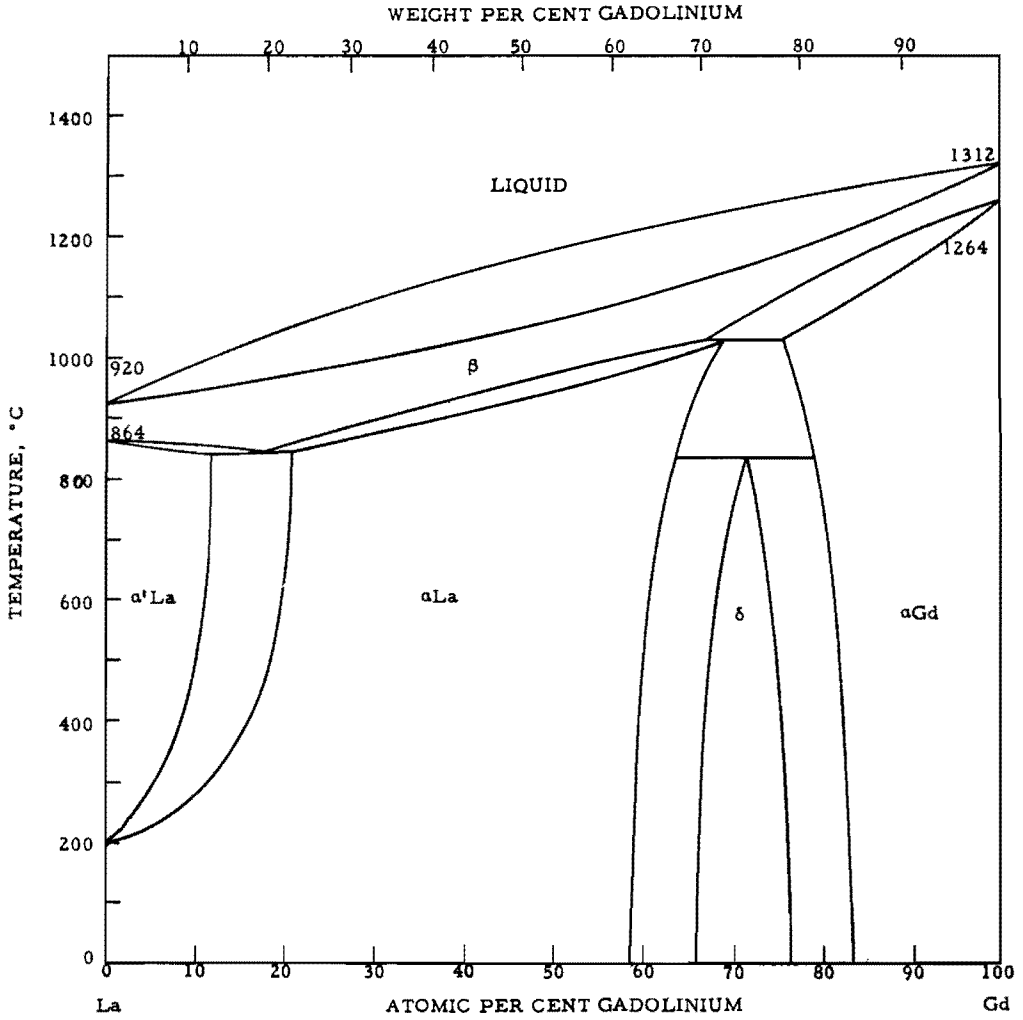

Figure 2. The Equilibrium Phase Diagram, Lanthanum-Gadolinium

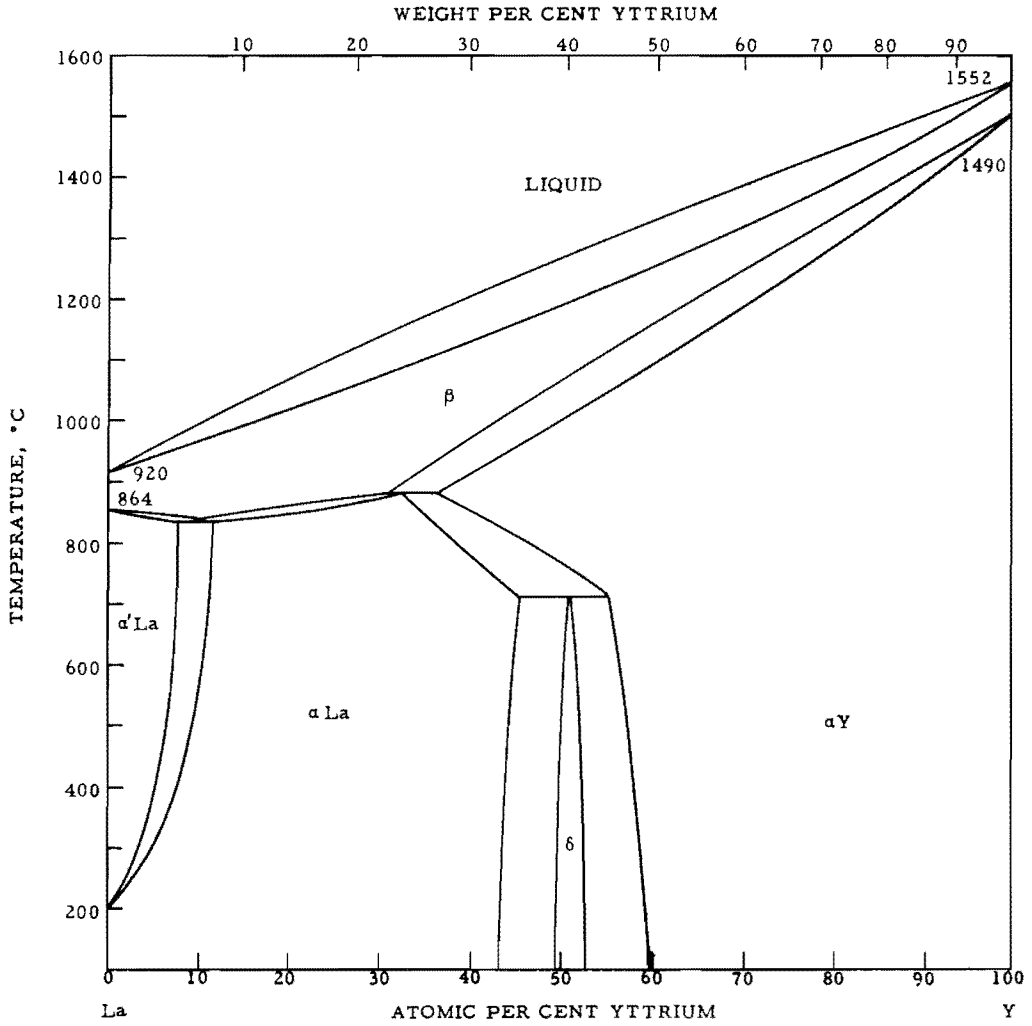

Figure 3. The Equilibrium Phase Diagram, Lanthanum-Yttrium

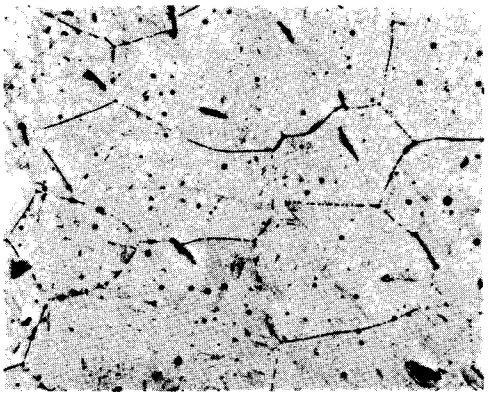

Figure 4. The as-cast structure of lanthanum metal. Impurity phase is oxide.

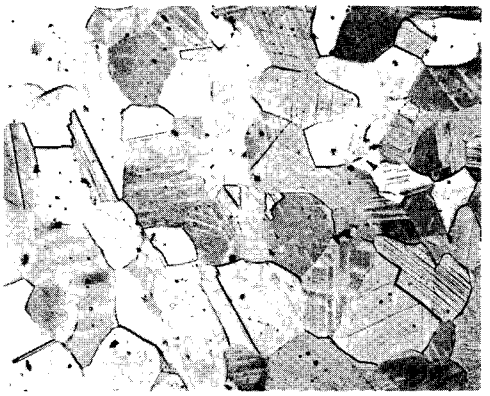

Figure 5. The as-cast structure of cerium metal.

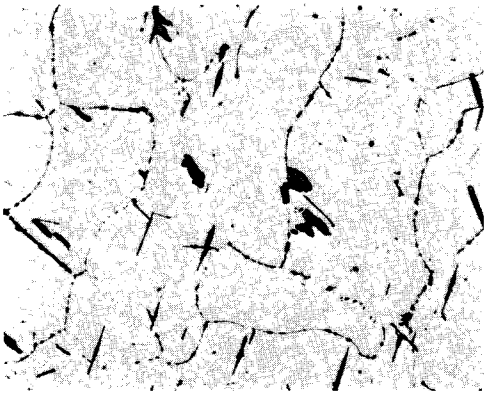

Figure 6. The as-cast structure of neodymium metal. Impurity phase is oxide.

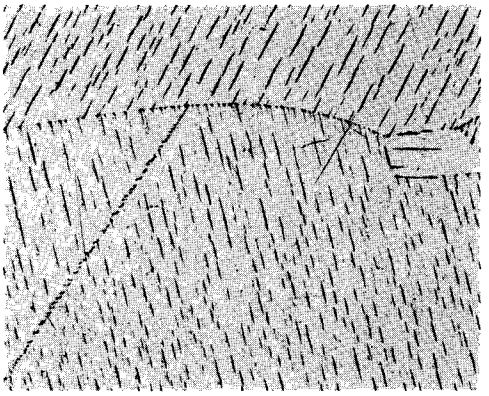

Figure 7. The as-cast structure of gadolinium metal. Minor oxide phase present.

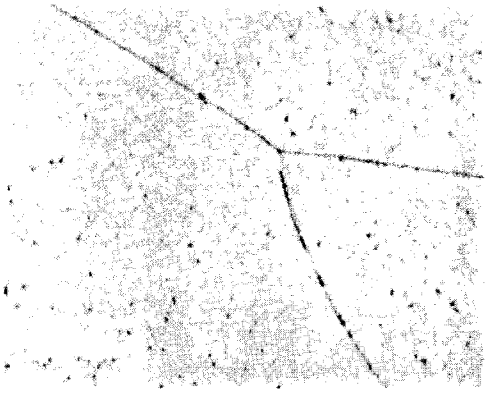

Figure 8. The as-cast structure of holmium metal. Minor oxide phase present. 250X

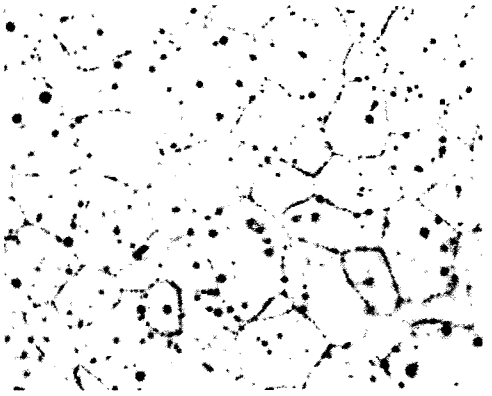

Figure 9. The as-cast structure of lutetium metal. Minor oxide phase present 250X

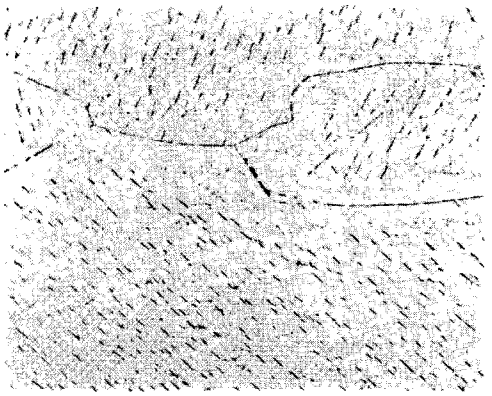

Figure 10. The as-cast structure of yttrium metal. Minor oxide present. 250X

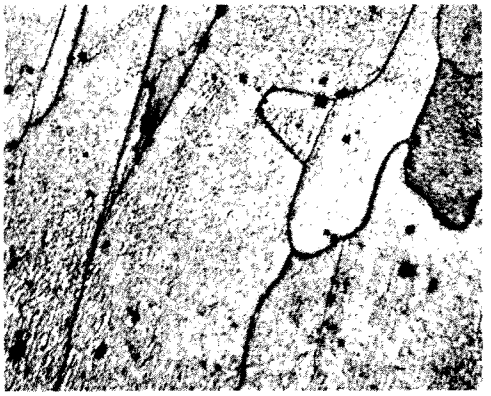

Figure 11. The as-cast structure of scandium metal. Oxide phase present. 250X

cerium, and neodymium were particularly difficult to prepare to obtain a clearly defined microstructure. The problem was in maintaining a surface, free of reaction product in the final stages of polishing and etching. These materials are extremely reactive. The minor phase which appears in all the metals at grain boundaries and within the grains is the oxide phase. At high magnifications it can be easily identified by its characteristic grey non-metallic appearance. It generally tends to be platelike and follow certain crystallographic directions, as can be readily seen in the yttrium and gadolinium. Figure 12 is the structure of pure samarium metal which was obtained for comparison with the samarium-type intermediate phases found in the binary systems. The very fine striations and banding, established to be twinning, are very characteristic of the samarium-type phase in the alloys. The microstructure of samarium metal will be discussed more fully later.

The observed microstructures throughout any system exhibiting the samarium-type structure can be represented by any one of the systems. This is to say that the microstructures are absolutely identical from one system to the next, except that their relative position in the system shift depending on which system is involved. The Nd-Gd system will be used to represent the microstructural morphology of this general class of light-heavy, rare-earth binary systems.

As one proceeds from the neodymium-rich region to the gadolinium-rich region, the first microstructure observed is the neodymium-rich solid solution. This structure is presented in Figure 13*, which is of a 20 a/o Nd alloy. Equiaxed grains are present, characteristic of most of the solid solution alloys. In Figure 14 of a 30 a/o Nd alloy, the solid solution still persists. At 40 a/o Nd, the first "precipitate" of the samarium-type structure or phase was observed, as pictured in Figure 15. This new phase has developed from the solid-solution matrix and has all of the characteristics of supersaturation. Grains of this new phase are easily recognized by several distinctive characteristics. First, they etch much darker than the matrix phase due to the fine striations or banding, which is attributed to microtwinning. Evidence confirming the presence of twins will be produced in a subsequent section. Second, the crystallographic

* The structures represented throughout the report are of homogenized alloys unless otherwise specified.

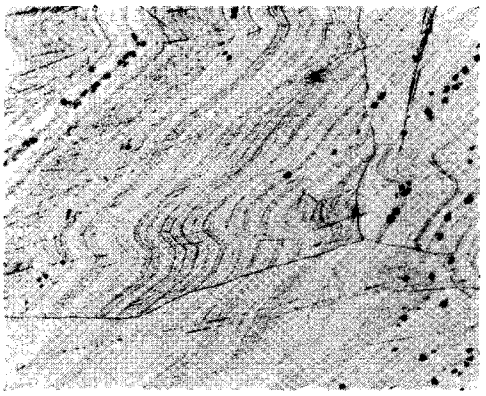

Figure 12. The as-cast structure of samarium metal. Note microtwin striations. 250X

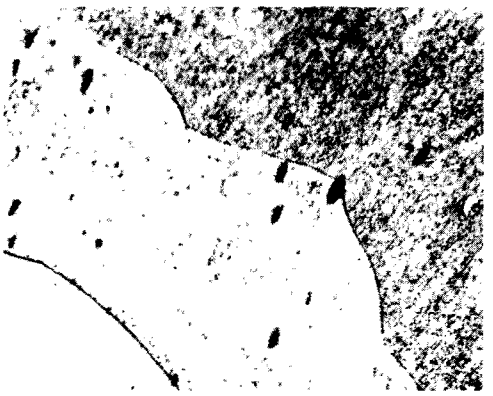

Figure 13. The homogenized structure of a 20 a/o Nd-80 a/o Gd alloy in the solid-solution region. 250X

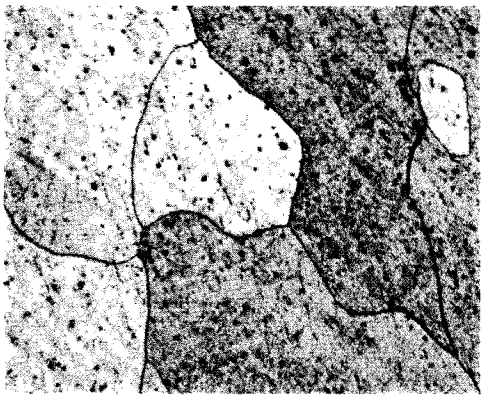

Figure 14. The homogenized structure of a 30 a/o Nd-70 a/o Gd alloy in the solid-solution region. 250X

Figure 15. The homogenized structure of a 40 a/o Nd-60 a/o Gd alloy, showing the first platelets of samarium-type phase. Note the microtwinning in the new phase. 250X

morphology is unique, in that, these new grains appear to have formed from the matrix in definite crystallographic directions. When they appear as the minor phase, they are elongated, usually parallel to the direction of the twin markings. Third, the samarium-type phase is separated from the matrix by incoherent boundaries, indicative of a major orientation difference between the matrix and the nucleating phase. The sides of the grains are almost always parallel to the markings. The grains are enclosed at either end by boundaries with no particular orientation relationship. This feature is illustrated by Figure 16, the microstructure of a 65 a/o Nd alloy in the Nd-Ho system. The nucleation and growth of these grains have the character of a shear-type phenomena, with the growth in the direction of the twin markings. Thus, it is thought that growth is propagated by a twinning mechanism. In some cases the grains will nucleate and grow across a prior matrix grain boundary, completely obliterating the boundary within the grain. This feature is illustrated in Figure 17 of a 40 a/o Nd- 60 a/o Gd alloy. X-ray diffraction analysis of an alloy with mixed phases, such as that observed in Figure 17, gave two discrete sets of lines, one indexing to the matrix-solid-solution structure and the other to the samarium-type structure. It was these factors which earlier led one to the seemingly obvious conclusion that a two-phase field existed in this region, consisting of the terminal solid solution and a unique samarium-type intermediate phase. As one progresses through this compositional region of the system, the amount of matrix phase decreases and the twinned structure increases. The microstructure of a 50 a/o Nd alloy is observed in Figure 18. The entire alloy has been "transformed" to the grains of the samarium-type structure. This was earlier presumed to be the position of the intermediate phase. Again, X-ray diffraction analysis resulted in no trace of the neodium solid solution and a strong pattern of the samarium-type structure. The impingement of the samarium-type phase grains on one another is very interesting. The impression again is that the growth of the phase is rapid and unidirectional, parallel to the twins. Figure 19 of a 34 a/o La-66 a/o Gd alloy demonstrates the grossly serated boundaries at the ends of the twinned grains, as if they grew in this direction. These high-energy boundaries would probably straighten out if they had been formed by slow growth, uniform in all directions. The appearance of the microstructure in Figure 19 is suggestive of a shear-type structure. Figure 20 is the structure of a 60 a/o Nd alloy, in which the structure is beginning to coarsen. At 65 a/o Nd, the twin bands are even coarser, but their definition and resolution becomes rather diffuse, as pictured in Figure 21. The gadolinium solid solution is well developed at 70 a/o Nd, as seen in Figure 22. The impression

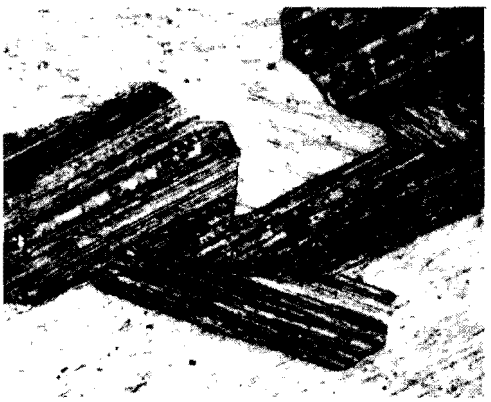

Figure 16. A 65 a/o Nd-35 a/o Ho alloy. Homogenized. Grains of samarium-type phase developed from the matrix. 250X

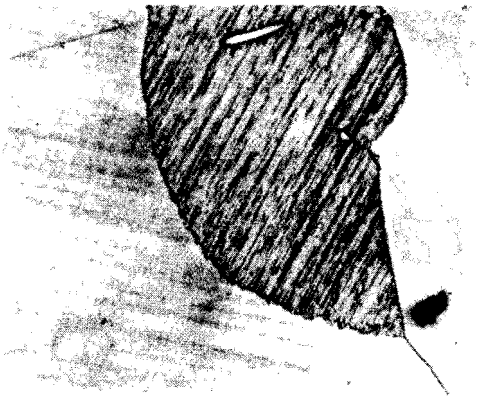

Figure 17. A 40 a/o Nd-60 a/o Gd alloy, homogenized. Samarium-type phase growing across the original matrix solid solution boundary. 500X

Figure 18. A 50 a/o Nd-50 a/o Gd alloy. Homogenized. Structure all samarium-type phase. 250X

Figure 19. A homogenized alloy of 34 a/o La-66 a/o Gd. All samarium-type phase. Illustrating serrated boundaries on impingement of grains in direction of growth. 250X

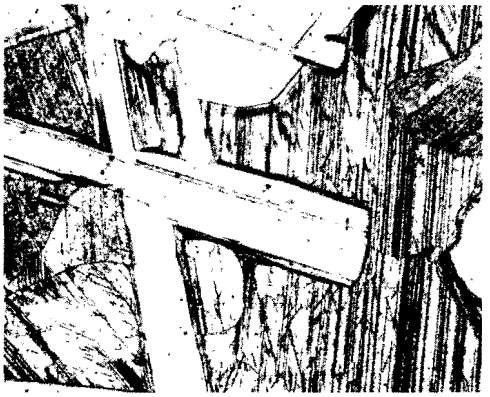

Figure 20. The homogenized structure of a 60 a/o Nd-40 a/o Gd alloy. Coarsening beginning. 250X

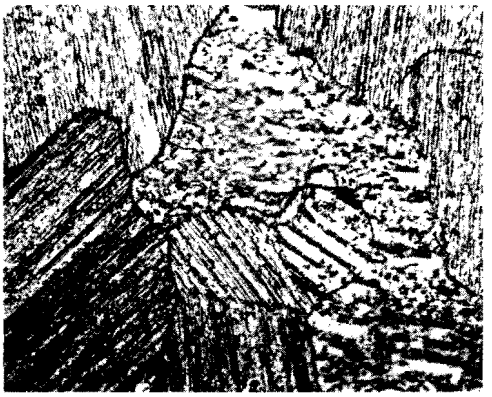

Figure 21. An alloy of 65 a/o Gd, homogenized. Coarsening progresses. Note diffuse twinned structure.

Figure 22. The homogenized structure of a 70 a/o Nd-30 a/o Gd alloy. Gadolinium solid solution present. 250X

Figure 23. A 64 a/o La-36 a/o Lu alloy. Homogenized. Structure thought to consist of two phases, La solid solution plus Lu solid solution. 250X

of crossing a solubility boundary in the observation of microstructures is not as clear cut at the gadolinium-rich end as the neodymium-rich end. This is generally true of all the systems, the light-rare-earth-rich boundary between the solid solution and the samarium-type phase is distinct, whereas the heavy-rare-earth-rich solid solution blends into the twinned structure gradually. One can never observe precipitate grains of the samarium structure in the heavy-rare-earth-rich region coming out of the matrix solid solution. The width of the region where the structure is 100 a/o samarium-type phase is difficult to determine; however, it is felt to be less than 5 a/o for any of the systems.

The possibility of the twins in the samarium-type phase being formed due to strains developed due to metallographic cold work was considered. After considerable experimentation with very careful polishing techniques, this idea was disproved. Electropolishing of the surface of a freshly arc melted button revealed much the same structure. The strains introduced into this specimen could come only from the composition region and/or the cooling rate.

The placement of the range of stability of the metallographically observed samarium-type phase was similarly accomplished for the other light-heavy rare earth binary systems. These data are summarized in Table IV.

Only four out of the thirteen systems did not unequivocally exhibit the samarium-type phase. The Gd-Sc and La-Sc systems were not expected to conform to the criteria of samarium phase formation, because scandium does not act like one of the rare earths. The La-Lu and Nd-Lu systems are in doubt as to whether they form the samarium-type phase. X-ray diffraction analysis did not definitely confirm the existence of the samarium structure in these systems, but the evidence for the presence of two phases is good. Metallographic analysis produced a range of compositions in each system, La-Lu and Nd-Lu, with a fine acicular, banded structure; somewhat different than observed in the other characteristic systems. Due to the difficulties in melting and homogenizing these specific alloys (described in the Experimental Section), the microstructures are not clear-cut. There is a distinct possibility that a two-phase region exists, consisting of the two terminal solid solutions rather than the presence of the samarium-type phase. The characteristic structures in the complex regions and the solid solution regions are presented in Figure 23 through 26. Figure 23 is the microstructure of a 64 a/o La - 36 a/o Lu alloy in

TABLE IV

Compositional Range of the Samarium-Type Phase

System	Light Rare Earth Boundary	Heavy Rare Earth Boundary	100% Samarium-Type Structure	Predicted Samarium-Type Structure
La-Gd	18 a/o La	40 a/o La	30 a/o La	29 a/o La
La-Y	40 a/o La	65 a/o La	52 a/o La	47 a/o La
La-Ho	45 a/o La	60 a/o La	55 a/o La	50 a/o La
La-Lu		Immiscibility Gap		
La-Sc		Immiscibility Gap		
Ce-Gd	25 a/o Ce	35 a/o Ce	30 a/o Ce	33 a/o Ce
Ce-Y	42 a/o Ce	68 a/o Ce	55 a/o Ce	54 a/o Ce
Ce-Ho	45 a/o Ce	60 a/o Ce	55 a/o Ce	55 a/o Ce
Nd-Gd	40 a/o Nd	60 a/o Nd	50 a/o Nd	50 a/o Nd
Nd-Y	55 a/o Nd	75 a/o Nd	65 a/o Nd	64 a/o Nd
Nd-Ho	60 a/o Nd	75 a/o Nd	70 a/o Nd	71 a/o Nd
Nd-Lu		Immiscibility Gap		
Gd-Sc		Complete Solid Solubility		

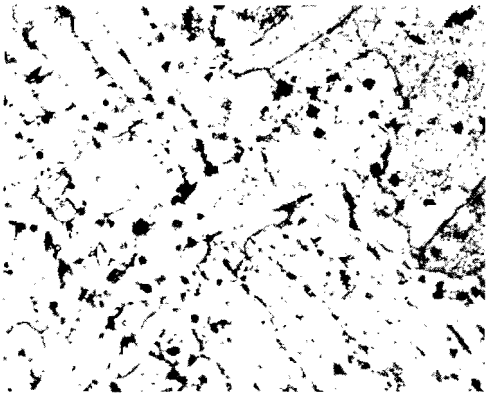

Figure 24. A 90 a/o Nd-10 a/o Lu alloy. Homogenized. Neodymium solid solution. 250X

Figure 25. The homogenized structure of an 82 a/o Nd-18 a/o Lu alloy. Two-phase region. 250X

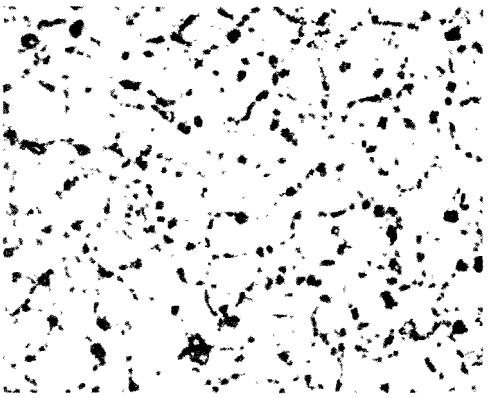

Figure 26. A 60 a/o Nd-40 a/o Lu alloy. Homogenized. Lutetium solid solution. 250X

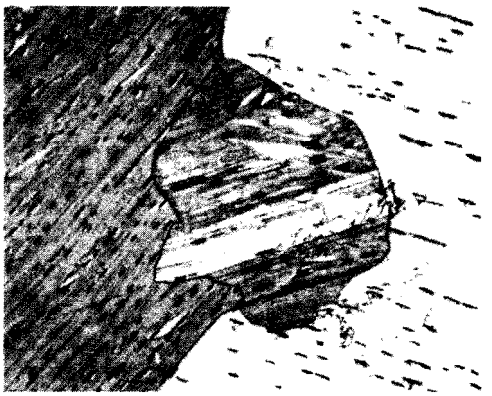

Figure 27. Pure samarium metal. As cast. Fine striations attributed to microtwins. 250X

the complex region. Figure 24 shows the neodymium solid solution structure of a 90 a/o Nd - 10 a/o Lu alloy. Figure 25 is the intermediate composition range where the structure is complex in a 82 a/o Nd - 18 a/o Lu alloy. The lutetium solid solution is observed in Figure 26 for a 60 a/o Nd - 40 a/o Lu alloy. As can be seen, the complex structure has a different appearance compared to the samarium-type structure.

Note from Table IV that the average compositional range of existence of the samarium-type phase is 20 a/o, ± about 5 a/o. Also, the composition at which the metallographic structure is completely composed of the samarium-type phase is estimated and tabulated. This composition in each alloy system conforms to one of the original hypotheses that the position of the samarium-type phase is predictable. The calculated positions of the samarium type structure are included in Table IV for comparison with the actual positions. Very good agreement is observed. If it is assumed that samarium metal is a transition between the light and heavy rare earths in structure because of size effect, then using a lever rule approach between the atomic numbers involved would give an estimate of the relative position of the samarium-type phase in an alloy system. The reason the lever rule is operative in this manner is because the atomic diameters of the elements are nearly linear as a function of atomic number. Since these alloy systems are random solid solutions, one finds a transition region in which the average distance between atoms (or average atomic diameter) is similar to that of pure samarium. The conditions for the formation of the unusual crystal structure are thus favorable.

Not only are the crystal structures of samarium metal and the alloy phase identical (or the packing sequence), but their microstructural morphologies are very similar in appearance. The characteristic microtwinning is present in both. Specimens of pure samarium metal from several different sources were metallographically analyzed. A survey of these proved that almost any structure seen in the alloys containing the samarium phase could be found in the pure metal. A few examples of these are presented in Figures 27 through 29. Note that the oxide phase precipitates out on the same habit planes as the microtwins.

In order to strengthen the premise that the complex phase equilibria first reported do not exist, a study by anneal-and-quench techniques was undertaken to determine whether the microstructures changed as a function of temperature. Two representative systems

Figure 28. Pure samarium metal. As cast. Fine striations attributed to microtwins. 250X

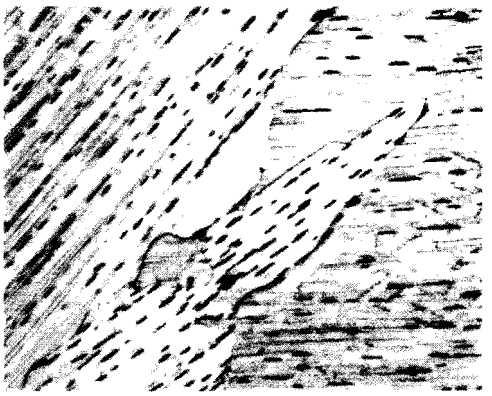

Figure 29. Pure samarium metal. As cast. Fine striations attributed to microtwins. 250X

Figure 30. A 50 a/o Nd-50 a/o Gd alloy. Homogenized, cold worked, annealed at 1000°C. 250X

Figure 31. A 50 a/o Nd-50 a/o Gd alloy. Homogenized, cold worked, annealed at 800°C. 250X

were selected for this study, the La-Gd and Nd-Gd systems. The anneal-and-quench technique allows one to detect the temperature level of an univariant reaction such as the peritectoid reaction, which was proposed to explain the mode of formation of the so-called delta phase. Temperature levels were selected over a large range of temperatures so as to bracket the univariant reaction, if it did in fact exist. An abrupt change in the characteristics of the structures quenched rapidly and observed at room temperature would be seen from those specimens annealed just above and just below the reaction isotherm. The range of alloy compositions were those which bracket the samarium-type structure region. The annealing schedule is presented in Table V.

As a result of observing and analyzing the microstructures from these anneals, the general conclusion was that no peritectoid reaction level could be detected. There was no significant changes in microstructure as a function of temperature. Another series of alloys in the Nd-Gd system was prepared for an anneal-and-quench technique at 900° C for 6 hr. employing a high vacuum furnace with fast quenching capabilities. The specimen in this furnace can be quenched in situ by impinging a blast of helium on the specimen. The rate of cooling is extremely fast. On observing these specimens by metallography, much the same structures were seen as with the slower quenches. In these experiments a slight shift was noted in the range of existence of the samarium phase toward the heavy rare-earth region. In several cases in both systems, a very clear, single-phase structure was observed from alloys quenched from the center of the range of existence. The impression from these structures was that there may be a region at high temperature where no microtwinning is present. This would imply that the microtwinning occurs distinctly below and apart from the transformation from body-centered-cubic to hexagonal close packed. It had been formerly thought that the microtwinning occurred from the strains due to this transformation. However, definite proof on just where in the hexagonal close packed solid solution the microtwinning occurs is not available from any of these studies.

Another experiment was conducted by metallographic techniques to shed more light on the morphology of the samarium-type phase. It was thought that specimens could be severely cold worked and then raised to various elevated temperatures to determine what recrystallized structures would look like. Specimens from the La-Gd and Nd-Gd systems were selected at the 100% samarium-type structure position. They were cold worked to an 80% reduction by cold rolling

TABLE V

Annealing Schedule of the La-Gd and Nd-Gd Systems

Alloys	As-Cast	400C	600C	800C	825C	850C	815C	900C	950C	1000C	1100C	1150C
16 a/o La - 84 a/o Gd	--	--	--	150 hr	48 hr	48 hr	48 hr	48 hr	16 hr	--	--	--
18 a/o La - 82 a/o Gd	--	--	--	150	48	48	48	48	16	--	--	--
20 a/o La - 80 a/o Gd	--	--	--	150	48	48	48	48	16	--	--	--
28 a/o La - 72 a/o Gd	--	--	--	150	48	48	48	48	16	--	--	--
32 a/o La - 68 a/o Gd	--	--	--	150	48	48	48	48	16	--	--	--
36 a/o La - 64 a/o Gd	--	--	--	150	48	48	48	48	16	--	--	--
40 a/o La - 56 a/o Gd	--	--	--	150	48	48	48	48	16	--	--	--
44 a/o La - 56 a/o Gd	--	--	--	150	48	48	48	48	16	--	--	--
50 a/o La - 40 a/o Gd	--	--	--	150	48	48	48	48	16	--	--	--
70 a/o Nd - 30 a/o Gd	X	400 hr	200 hr	16 hr	--	--	--	6 hr	--	8 hr	2 hr	1/2 hr
65 a/o Nd - 35 a/o Gd	X	400	200	16	--	--	--	6	--	8	2	1/2
60 a/o Nd - 40 a/o Gd	X	400	200	16	--	--	--	6	--	8	2	1/2
55 a/o Nd - 45 a/o Gd	X	400	200	16	--	--	--	6	--	8	2	1/2
50 a/o Nd - 50 a/o Gd	X	400	200	16	--	--	--	6	--	8	2	1/2
45 a/o Nd - 55 a/o Gd	X	400	200	16	--	--	--	6	--	8	2	1/2
40 a/o Nd - 60 a/o Gd	X	400	200	16	--	--	--	6	--	8	2	1/2
35 a/o Nd - 65 a/o Gd	X	400	200	16	--	--	--	6	--	8	2	1/2
30 a/o Nd - 70 a/o Gd	X	400	200	16	--	--	--	6	--	8	2	1/2

and annealed at 1000, 800, 600, and 400° C, respectively. Immediately after the anneal the samples were rapidly quenched to toom temperature. The as-worked structure was exceedingly difficult to etch because it was so dense with mechanical twins. The annealed structures still showed microtwinning, but was either coarse at the higher temperatures or fine at the lower temperatures. Recrystallization probably occurred, but the microtwins were still present in the new grains. Figures 30 through 32 show the structures of a 50 a/o Nd-50 a/o Gd alloy cold worked and annealed at 1000, 800, and 600° C, respectively.

Electron micrography was used to look at the structures of the samarium-type phase. Not much additional information was gained that could not already be obtained by observations from the optical microstructures. Figure 33 is the structure of a 55 a/o Nd - 45 a/o Gd alloy at a magnification of 2300.

In summary, the metallographic analysis of intra-rare-earth binary systems established that these systems have complete solid solubility in the low temperature, hexagonal-close packed modification (and undoubtedly in the high-temperature body-centered-cubic form). However, as one proceeds across the solid solution from light rare earth to heavy rare earth, a transition region in stacking sequence occurs with the appearance of newly formed grains, whose formation is apparently dependent on strain considerations. Apparently, the heavy-and light-rare-earth, solid-solution stacking sequences are not compatible in a gradual changeover from one to the other in the alloy system, and a region in between must be present to accommodate the strain's set up. The reason this is true in these alloys is felt to be the same reason that pure samarium metal is a transition between the light-and heavy-rare-earth elements. The new grains are formed from the matrix with no change in composition; (from electron-beam microprobe analysis described in next section) thus, the phenomenon is a recrystallization-type reaction. Furthermore, the recrystallization involves a microtwinning mechanism which is closely associated with the nucleation and growth of the new grains. The twinned alloy grains are identical in both morphology and crystal structure (as will be seen in the next section) with pure samarium. The range of existence of the samarium-type phase averages about 20 a/o in these systems. This range of existence changes for the particular system, being predictable on the basis of size factors of samarium and the two component metals. The relative amount of the new grains is composition dependent. The onset of this precipitation from the light-rare-earth solid solution is very reproducible, composition-wise. This would not be unexpected,

Figure 32. A 50 a/o Nd-50 a/o Gd alloy. Homogenized, cold worked, annealed at 600°C. 250X

Figure 33. Electron micrograph of at 55 a/o Nd-45 a/o Gd alloy. Homogenized. 2300X

because the new grains with the samarium structure are thought to be size factor dependent. As one proceeds toward the heavy-rare-earth region, the amount of the samarium-type structure increases until all of the matrix has been transformed to the new structure at some intermediate position within the 20 a/o range. From here on the twinning coarsens, and the composition at which the samarium-type structure is no longer present and the heavy-rare-earth solid solution has completely evolved in very diffuse and indefinite. The "boundary" is not as distinct as the light-rare-earth extreme of the range of existence of this phase. Finally, one of the most interesting aspects of this study is that one can effectively "synthesize" samarium metal, both in morphology and structure, by alloying a light rare earth with a heavy-rare-earth.

C. X-Ray Structure Analysis

The objective of this phase of study was to provide a complementary method to metallographic analysis, so that a more complete confirmation of the structural characteristics of the selected intra-rare-earth binary systems could be made. X-ray diffraction analysis employing film techniques were conducted on the alloys of interest to determine, first, the type of structure, and, second, the lattice parameters. A detailed description of the techniques was presented in the Experimental section. The types of structures that were sought were limited to three possible hexagonal-close-packed modifications, involving changes only in the stacking sequence. The three types are best described pictorially as presented in Figure 34. The light-rare-earths are the La type (A3'), the heavy-rare-earths the Mg type (A3), and samarium is the Sm type. The three types of solid solutions throughout each alloy system have the same types of structures.

Preliminary to investigating the samarium-type structures in the alloys, the lattice parameters and X-ray and observed densities of the pure constituents were determined (lutetium and scandium were omitted). Table VI presents the data on the pure metal; lanthanum, cerium, neodymium, samarium, gadolinium, yttrium, and holmium.

X-ray diffraction studies of alloys of nine systems have been conducted throughout the course of this program. In Tables VII through XV the structural parameters are presented. Comparing the composition ranges of the samarium-type structure by X-ray diffraction techniques compares favorably with the metallographic data in

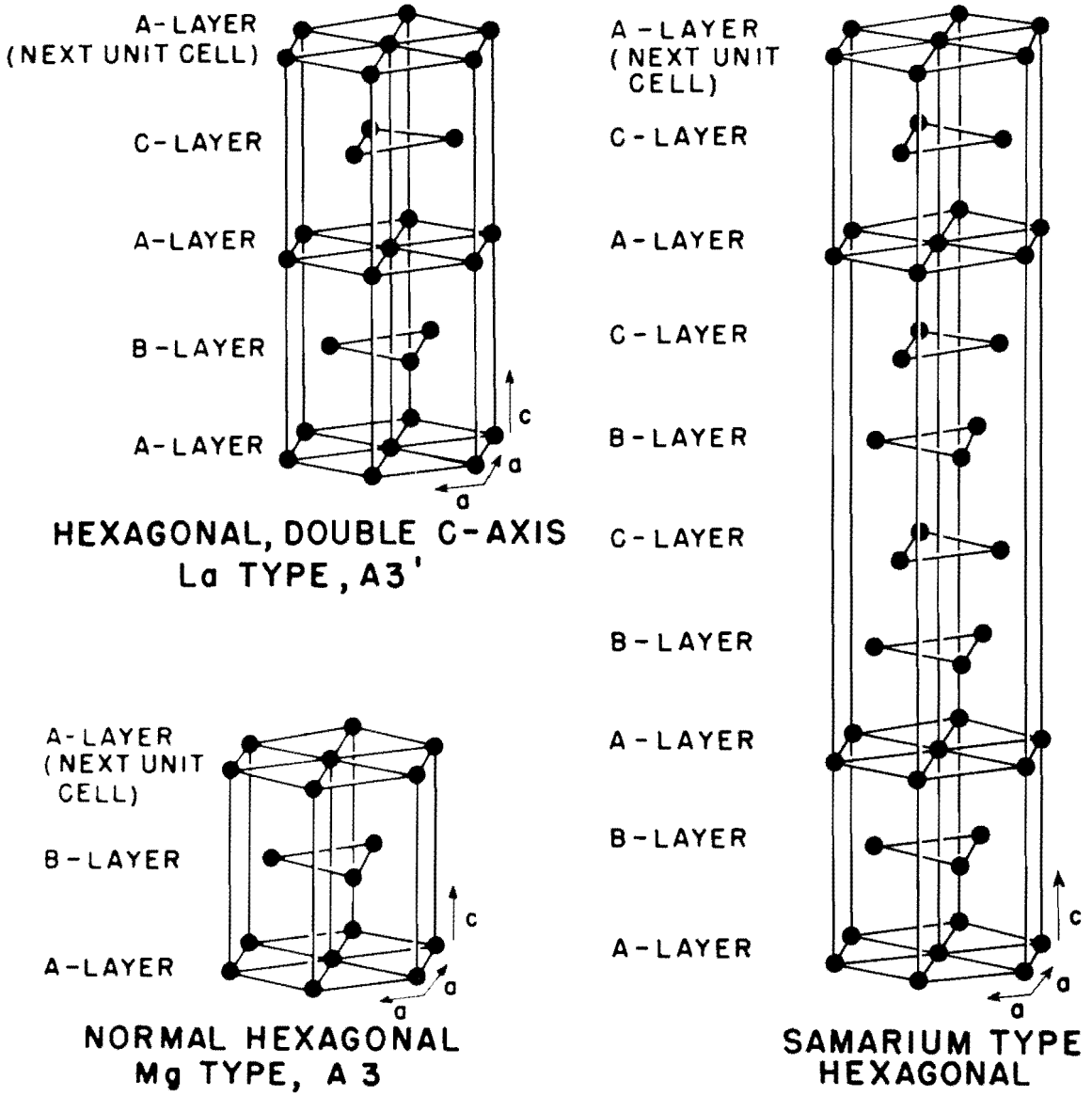

Figure 34. The Crystallographic Structures of the Three Types of Closest Packing of Spheres Observed in Rare Earth and Related Metals.

TABLE VI

Lattice Constants and Densities of the Pure Intra-Rare-Earth Components and Samarium

Element	Pycnometric Density (gm/cm^3)	X-Ray Density (gm/cm^3)	Lattice Constants (Å)			Lattice Constants after Herrmann,[5] et al.		
			a_o	c_o	c/a	a_o	c_o	c/a
Ce	6.77	6.773	5.1600	---	---	5.1612	---	---
La	6.17	6.150	3.7767	12.1445	1.608	3.770	12.159	1.613
Nd	7.00	7.003	3.6609	11.788	1.610	3.6579	11.7992	1.613
Sm	7.50	7.572	3.6215	26.136	1.605	3.621	26.25	1.611
Gd	7.88	7.932	3.6285	5.7739	1.591	3.6360	5.7826	1.590
Y	4.49	4.491	3.6275	5.7688	1.590	3.6474	5.7306	1.571
Ho	8.77	8.788	3.5732	5.6100	1.570	3.5773	5.6158	1.570

TABLE VII

Lattice Constants and Densities of La-Gd Alloys

Composition a/o La	Pycnometric Density (gm/cm^3)	X-Ray Density (gm/cm^3)	Solid Solution Phase			Samarium Phase		
			a_o(A)	c_o(A)	c/a	a_o(A)	c_o(A)	c/a
10	7.71	7.714	3.6426	5.8100	1.597	--	--	--
12	7.66	7.677	3.6482	5.8071	1.592	--	--	--
14	7.62	7.637	3.6513	5.8139	1.592	--	--	--
16	7.67	7.598	3.6540	5.8215	1.593	--	--	--
18	7.64	7.568	3.6545	5.8292	1.595	--	--	--
20	7.56	7.550	3.6534	5.8326	1.596	--	--	--
22	7.50	7.494	3.6557	5.8552	1.602	--	--	--
24	7.46	--	3.6531	5.8416	1.599	3.6498	26.106	1.590
26	7.43	--	3.6563	5.8549	1.601	3.6536	26.362	1.603
28	7.40	--	3.6342	5.8619	1.613	3.6589	26.446	1.606
30	7.34	7.363	--	--	--	3.6623	26.471	1.606
32	7.31	7.326	--	--	--	3.6638	26.518	1.608
34	7.27	7.286	--	--	--	3.6693	26.521	1.606
36	7.26	7.262	trace of 2nd phase present			3.6677	26.571	1.610
38	7.22	7.237	trace of 2nd phase present			3.6681	26.593	1.611
40	7.18	--						
42	7.16	--	Multiple phase materials. Films indicate that alpha,					
44	7.09	--	beta and gamma lanthanum structures are present.					
46	7.07	--	Films too complicated to permit full interpretation.					
50	7.00	--						
60	6.82	--						
30						3.667	26.482	1.605[2]

TABLE VIII

Lattice Constants and Densities of La-Y Alloys

Composition a/o La	Pycnometric Density (gm/cm^3)	X-Ray Density (gm/cm^3)	Solid Solution Phase			Samarium Phase		
			a_o(A)	c_o(A)	c/a	a_o(A)	c_o(A)	c/a
20	4.82	4.861	3.6640	5.8120	1.586	--	--	--
36	5.11	5.209	3.6859	5.8193	1.579	--	--	--
38	5.16	5.176	3.6928	5.8626	1.588	--	--	--
40	5.18	5.183	3.7058	5.8664	1.583	--	--	--
42	5.22	5.207	3.7021	5.9053	1.595	--	--	--
44	5.26	5.243	3.7063	5.9047	1.593	--	--	--
46	5.29	5.305	3.7016	5.9040	1.595	--	--	--
48	5.34	--	Poor resolution in back reflection region, 2 phases present					
50	5.37	5.382	--	--	--	3.7057	26.595	1.595
52	5.42	5.427	--	--	--	3.7045	26.624	1.597
54	5.43	--	Multiple phase material. Films indicate that alpha, beta and gamma lanthanum structures are present. Films too complicated to permit full interpretation.					
56	5.46	--						
58	5.49	--						
60	5.50	--						
70	5.68	--						
80	5.86	--						
47.9						3.699	26.70	1.604[2]

TABLE IX

Lattice Constants and Densities of La-Ho Alloys

Composition % La	Pycnometric Density (gm/cc)	X-Ray Density (gm/cc)	Solid Solution Phase			Samarium Phase		
			a_o(A)	c_o(A)	c/a	a_o(A)	c_o(A)	c/a
35	7.69	--	Insufficient lines		--	--	--	--
40	7.62	--	Insufficient lines		--	--	--	--
55	--	--	--	--	--	3.628	26.332	1.613
60	7.16	7.22	3.6683 ±.0027	11.7855 ± .0092	1.607	--	--	--
65	6.81	7.16	3.4990 ±.0020	11.210 ± .0094	1.602	--	--	--
70	6.79	6.94	3.6956 ±.0040	11.8644 ± .0140	1.605	--	--	--
75	--	--	Too many interfering lines					

TABLE X

Lattice Constants and Densities of Ce-Gd Alloys

Composition a/o Ce	Pycnometric Density (gm/cc)	X-Ray Density (gm/cc)	Solid Solution Phase			Samarium Phase		
			a_o(A)	c_o(A)	c/a	a_o(A)	c_o(A)	c/a
5	7.83	7.82	3.6388 ±.0007	5.7915 ±.0003	1.592	--	--	--
10	7.80	7.77	3.6398 ±.0008	5.7942 ±.0003	1.592	--	--	--
15	7.75	7.72	3.365 ±.021	5.816 ±.039	1.600	--	--	--
20	7.72	7.68	3.641 ±.004	5.793 ±.004	1.591	--	--	--
25	7.69	--	Insufficient lines			--	--	--
30	--	--	--	--	--	3.618	26.289	1.610
40	7.53		Insufficient lines			--	--	--
45	7.50	7.41	3.6118 ±.016	11.863 ± .0004	1.642	--	--	--
80	--	--	--	--	--	3.64	26.27	1.604[8]

TABLE XI

Lattice Constants and Densities of Ce-Y Alloys

Composition a/o Ce	Pycnometric Density (gm/cm^3)	X-Ray Density (gm/cm^3)	Solid Solution Phase			Samarium Phase		
			a_o(A)	c_o(A)	c/a	a_o(A)	c_o(A)	c/a
30	5.15	5.202	3.6596	5.7397	1.568	--	--	--
35	5.28	5.246	3.6688	5.8015	1.581	--	--	--
40	5.36	--	3.6640	5.7854	1.580	3.6555	26.163	1.590
42	5.44	--	3.6692	5.7868	1.577	3.6588	26.159	1.589
44	5.48	--	3.6637	5.8182	1.588	3.6577	26.249	1.595
46	5.51	--	3.6688	5.8318	1.590	3.6607	26.280	1.595
50	5.65	5.621	--	--	--	3.6521	26.355	1.604
55	5.73	5.768	--	--	--	3.6446	26.368	1.608
60	5.83	--	Multiple phase materials. Films too complicated to permit interpretation					
64	5.94	--						
66	5.97	--						
68	6.02	--						
70	6.07	--						
75	6.19	6.214	3.6604	5.8582	1.600	--	--	--
44.5						3.653	26.55	1.614[2]

TABLE XII

Lattice Constants and Densities of Ce-Ho Alloys

Composition a/o Ce	Pycnometric Density (gm/cc)	X-Ray Density (gm/cc)	Solid Solution Phase			Samarium Phase		
			a_o(A)	c_o(A)	c/a	a_o(A)	c_o(A)	c/a
35	7.81	8.12	3.5979 ±.0004	5.6994 ±.0004	1.584	--	--	--
40	7.75	--	Insufficient lines			--	--	--
45	--	--	--	--	--	3.636	26.227	1.603
70	7.20	7.43	3.6144 ±.0030	11.6579 ± .0017	1.612	--	--	--
75	7.06	7.33	3.5969 ±.0046	11.8324 ± .0127	1.645	--	--	--

TABLE XIII

Lattice Constants and Densities of Nd-Gd Alloys

Composition a/o Nd	Pycnometric Density (gm/cc)	X-Ray Density (gm/cc)	Solid Solution Phase			Samarium Phase		
			a_o(A)	c_o(A)	c/a	a_o(A)	c_o(A)	c/a
30	7.61	7.68	3.638 ±.024	5.786 ±.047	1.591	--	--	--
35	7.55	7.57	3.638 ±.029	5.841 ±.060	1.606	--	--	--
40	7.49	7.53	3.6471 ±.0005	5.8248 ±.0006	1.597	--	--	--
50	--	--	--	--	--	3.659	26.036	1.581
65	7.25	7.31	3.5382 ±.0526	12.4743 ± .0978	1.763	--	--	--
70	7.25	7.26	3.6386 ±.0001	11.8153 ± .0005	1.623	--	--	--

TABLE XIV

Lattice Constants and Densities of Nd-Y Alloys

Composition a/o Nd	Pycnometric Density (gm/cm^3)	X-Ray Density (gm/cm^3)	Solid Solution Phase			Samarium Phase		
			a_o(A)	c_o(A)	c/a	a_o(A)	c_o(A)	c/a
40	5.48	5.510	3.6645	5.7562	1.571	--	--	--
45	5.60	5.622	3.6680	5.7702	1.573	--	--	--
50	5.72	5.760	3.6679	5.7692	1.573	--	--	--
55	5.88	5.895	3.6666	5.7758	1.575	--	--	--
60	6.01	--	trace of second phase present			3.6466	26.316	1.604
65	6.14	6.228	--	--	--	3.6153	26.160	1.608
69	6.24	--	Poor resolution in back-reflection region, single phase					
70	6.27	6.246	--	--	--	3.6476	26.393	1.608
75	6.41	--	3.5251	11.6473	1.652	3.6277	26.318	1.612
80	6.54	--	Multiple phase material. Too complicated for interpretation					
85	6.66	6.734	3.6278	11.764	1.622	--	--	--
90	6.77	--	Poor resolution in back-reflection region, single phase					
95	6.89	6.934	3.6439	11.791	1.618	--	--	--
64.9						3.662	26.382	1.601[2]

TABLE XV

Lattice Constants and Densities of Nd-Ho Alloys

Composition a/o Nd	Pycnometric Density (gm/cc)	X-Ray Density (gm/cc)	Solid Solution Phase			Samarium Phase		
			a_o(A)	c_o(A)	c/a	a_o(A)	c_o(A)	c/a
50	7.79	--	Insufficient lines					
55	7.49	7.80	3.6296 ±.0035	5.7297 ±.0009	1.579	--	--	--
60	7.44	7.72	3.6305 ±.0001	5.7634 ±.0002	1.588	--	--	--
70	--	--	--	--	--	3.642	26.640	1.625
80	6.99	7.36	3.5504 ±.0048	11.3517 ± .0003	1.598	--	--	--
85	6.95	7.27	3.6442 ±.0089	11.7775 ± .0249	1.607	--	--	--

Table IV. Lattice parameters were not reported for specimens which did not give good resolution in the back-reflection region. The X-ray data from other investigations are included for comparison. Several additional alloys in other systems studied by X-ray diffraction analysis and not included in the Tables have the following samarium-type lattice parameters:

System	a/o	a_o	c_o	c/a
Pr-Y[2]	49.7 Pr	3.648	26.41	1.609
Nd-Tm[2]	63.0 Nd	3.656	26.36	1.602

Similar to the metallographic analysis, X-ray diffraction identification of the samarium-type phase recrystallizing out of the light-rare-earth solid solution was clear and concise. The situation in the heavy-rare-earth region of the overlap of the two structures was not well defined. It is interesting to note that the lattice parameters of the samarium-type phase change in an orderly manner from the light-rare-earth boundary to the heavy-rare-earth boundary, which is to be expected if this structure varies in composition within its range of existence. The c/a values also increase in an orderly fashion as the composition changes from light-to heavy-rare-earth-rich.

The two scandium-base systems were not analyzed by X-ray diffraction analysis since they did not show isomorphism with the other intra-rare-earth binary systems. A careful analysis of the La-Lu and Nd-Lu systems because of the metallographic differences observed in them compared to the other nine systems, resulted in the conclusion that a two-phase miscibility gap exists in these systems. An indexing was attempted to the samarium structure, but a reasonable fit was not obtained. A good indexing was, however, found for a lanthanum and lutetium solid solution in the La-Lu system. The same was true for the neodymium solid solutions in the Nd-Lu system, but the lutetium solid solution indexing was not reasonable.

The data were taken for the 34 a/o La - 66 a/o Lu alloy and the 77 a/o Nd - 23 a/o Lu. Both of these were selected on the basis of the two-phase character of their microstructures. The lattice parameters determined were as follows:

	34 a/o La - 66 a/o Lu Alloy			
	a_o(A)	c_o(A)	c/a	Density, gm/cc
La Solid Solution	3.727	12.028	1.613	7.466
Lu Solid Solution	3.547	5.642	1.590	8.787

	77 a/o Nd - 23 a/o Lu Alloy			
	a_o(A)	c_o(A)	c/a	Density, gm/cc
Nd Solid Solution	3.696	11.916	1.615	7.152
Lu Solid Solution	Interpretation not possible			

The proposed phase equilibria most probable to accommodate an immiscibility gap would be a eutectoid reaction of the high-temperature body-centered-cubic allotrope to lanthanum solid solution plus lutetium solid solution. The eutectoid composition would be very near the sample compositions above. Also, the width of the immiscibility gap appeared to be about 20 a/o from the metallographic analysis.

A key experiment, which was excellent direct evidence that the intermediate delta phase does not exist, inclusive of the associated two-phase fields to either side of the position of the delta phase, was electron-beam-microprobe analysis of the alloy structures. Two independent sources were requested to provide these services. One was the Materials Analysis Company of Palo Alto, California and the other, the Dow Chemical Company, Rocky Flats Plant, Boulder, Colorado. Samples were submitted of both the 18 a/o La - 82 a/o Gd alloy and the 40 a/o Nd - 60 a/o Gd alloy. These contained small amounts of the samarium-type structure in a matrix of the light-rare-earth solid solution, such as one observes in Figure 16. Traverses were made across the twinned grains and into the solid solution on either side. No compositional differences were detected in any of the traverses. If the peritectoid reaction existed, a discrete change in composition would have been detected between these two phases. However, since none were observed, the recrystallization phenomena is the only valid explanation wherein no compositional change is expected. The La Lα and Gd Lα radiations were both independently recorded for the La-Gd system, and the Nd Lα and the Gd Lα radiations were recorded for the Nd-Gd system. Figure 35 is a photograph of the chart recording showing one of the traverses. Table XVI presents the electron-beam microprobe conditions employed for the La-Gd system. The conditions for the Nd-Gd system were essentially the same.

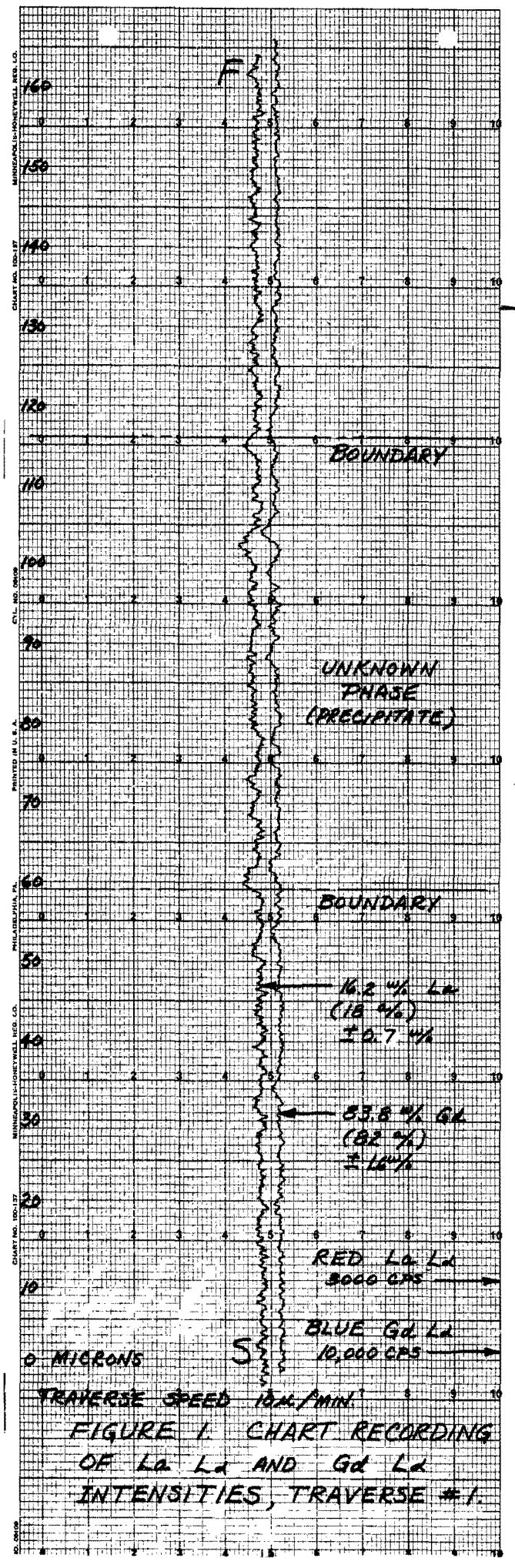

Figure 35. Electron-Beam Microprobe Chart Recordings.

TABLE XVI

Conditions Used in the Analyses

	La		Gd
High Voltage, KV		30	
Bias Resist., megohms		4	
Gun Current, μamps		80	
Accelerating Voltage, KV		29.7	
Aperture Diaphragm, in.		0.016	
Specimen Current, μamps		0.02	
Spectral Line Measured		Lα	
λ, Angstroms	2.665		2.046
Secondary Slit, in.		None	
Analyzing Crystal (cvd.)		LiF	
Detector:	FPC		SPC
Gas	P-10		Xenon
Pressure, atm.	1		1/2
Entrance Window	1/8 mil mylar		2 mil Be
Exit Window	1 mil mylar		2 mil Be
Voltage, v.		1350	
Amplification	1/16 × 0.5		1/16 × 0.8
Pulse Height Selector:		Differential	
Base Line, v		1.8	
Window, v		2.5	
Probe Diameter, microns		1.5	
Standard Used	LaO		GdO

Another fruitful experiment was conducted, employing high-temperature X-ray diffraction analysis. Since a peritectoid reaction was reported earlier, which is the mechanism proposed to form the samarium-type delta phase, the use of X-ray techniques to establish the absence or presence would be fruitful. An alloy at the proposed stoichiometric composition of the delta phase in the La-Gd system was selected. The composition was 30 a/o La - 70 a/o Gd. The diffractometer was set to oscillate on three of the major reflections from the samarium-type structure. The hexagonal indices were as follows; 009, 104, 105. A powder sample was prepared and loaded into the specimen holder of the MRC Manufacturing Corporation, high-temperature, high-vacuum X-ray diffractometer attachment. The attachment was employed with a Philips Wide-Range Goniometer. A platinum/platinum-13% rhodium thermocouple was used to sense the temperature.

The temperature was elevated in discrete steps and allowed to equilibrate. At each level, the presence and position of the three reflections were observed. They were present at all temperature levels up to 900° C. The peritectoid reaction was reported to occur at about 825° C.[2] The conclusion reached in this experiment was that the presence of the peritectoid level could not be confirmed. The samarium-type structure was found to exist up to 900° C.

Laue back-reflection analysis of single grains of various alloys was conducted from metallographic specimens. The objective was to determine whether twinning was responsible for the appearance of the striations. If the structure was twinned, the back-reflection pattern of Laue spots would show double reflections instead of single Laue reflections. The pattern did in fact demonstrate this configuration. Three specimens were analyzed; a 50 a/o Nd - 50 a/o Gd alloy with the samarium structure, a 30 a/o Nd - 70 a/o Gd alloy in the gadolinium-rich solid solution, and pure samarium metal. The 50 a/o Nd - 50 a/o Gd structure and pure samarium showed a pattern characteristic of twinning, whereas the 30 a/o Nd - 70 a/o Gd alloy did not exhibit this effect. In conjunction with the microstructural appearance, the evidence is very convincing that the samarium-type phase is microtwinned.

D. Auxiliary Data

During the course of this investigation it was thought that a multiphased experimental program was necessary to produce incontrovertible clarification of the nature of the intra-rare-earth

binary systems. In addition to metallography and X-ray diffraction analyses, other techniques were invoked which included thermal analysis, resistivity, dilatometry, density, and hardness. The thermodynamic studies were different in nature and objective, and thus will be discussed in a subsequent section.

The techniques employed in this portion of the overall study were applied to specimens in which the samarium-type phase existed. Whether this phase was formed by a peritectoid reaction versus a recrystallization phenomenon was the goal. The problem was to establish whether the reaction isotherm could be detected. This would require experiments which employed the determination of some basic property of the alloy as a function of changing temperature. Thermal analysis, and resistivity were the most logical tools. Nine of the binary systems were selected to conduct the experiments. The compositions of the systems that most nearly approached 100% samarium-type structure were analyzed. The systems and their compositions are presented in Table XVII.

TABLE XVII

Samarium-Type Structures Studied By Thermal Analysis and Resistivity

Alloy Composition
100% Nd
30 a/o La - 70 a/o Gd
52 a/o La - 48 a/o Y
50 a/o La - 50 a/o Ho
33 a/o Ce - 67 a/o Gd
55 a/o Ce - 45 a/o Y
55 a/o Ce - 45 a/o Ho
50 a/o Nd - 50 a/o Gd
71 a/o Nd - 29 a/o Ho
70 a/o Nd - 30 a/o Ho

The pure neodymium specimen was used to calibrate the equipment and determine its sensitivity. The solid-state transformation was clearly indicated by a thermal arrest in the case of thermal analysis and a discrete change in resistivity with the resistivity apparatus at 851° C. This was reproducible on heating or cooling. A value of 862° C is reported in the literature[6]; minor impurities are attributed to the difference.

Each alloy was analyzed at least three times on each apparatus by raising and lowering the temperature through the range of interest. The results were negative in both the thermal analysis and resistivity. No inflections, indicative of a univariant reaction, could be detected. This confirms the previous experimental findings that the phenomenon under study is a special type of recrystallization based on a twinning mechanism.

Four samples were concurrently sent to the Los Alamos Scientific Laboratories to run on their dilatometer and differential thermal analysis apparatuses, since these have been developed to a very high degree of sensitivity. Some weak inflections were noted, but they were too inconsistent and did not correlate by any reasonable justification to either recrystallization or first-order phase equilibria.

Finally, hardness and density measurements were conducted on most of the samples that were subsequently microstructurally analyzed. The density and hardness data are presented in Table XVIII. These data were obtained to determine whether the phase boundaries and the proposed intermediate phase could be detected by distinctive trends in the hardness or density versus composition curves throughout each system. Figure 36 and 37 are plots of these curves respectively for the Nd-Gd system. The plots for all the other systems are identical in shape. The density plots are almost linear across each system. The hardness data show a general rise from each component to a maximum which always occurs in the light-rare-earth-rich region. This maximum had no relationship to the position of the samarium-type phase. The plots presented are typical of what one would expect for complete solid solubility, which is the case. Therefore, these data confirm the findings by the other techniques.

E. Thermodynamic Analysis

The objective in this final phase of study was to determine the thermodynamic properties in several representative binaries of the intra-rare earth systems. The three alloy systems chosen were the La-Gd, Nd-Gd and Hd-Ho systems, and were selected because they had been more thoroughly studied by other complementary experimentation, and would lend better to intercorrelation of data.

TABLE XVIII

Hardness and Density Data for the Binary Systems

La-Gd		
a/o La	DPH	gm/cc
10	--	7.71
12	--	7.66
14	--	7.62
16	--	7.67
18	--	7.64
20	--	7.56
22	--	7.50
24	--	7.46
26	--	7.43
28	--	7.40
30	--	7.34
32	--	7.31
34	--	7.27
36	--	7.26
38	--	7.22
40	--	7.18
42	--	7.16
44	--	7.09
46	--	7.07
50	--	7.00
60	--	6.82

La-Ho		
a/o La	DPH	gm/cc
30	65.3	7.74
35	64.5	7.69
40	62.9	7.62
42.5	--	7.22
45	63.8	7.54
47.5	--	7.14
50	56.1	7.43
55	59.1	7.30
60	52.0	7.16
65	46.4	6.81
70	43.6	6.79

La-Y		
a/o La	DPH	gm/cc
20	--	4.82
36	--	5.11
38	--	5.16
40	--	5.18
42	--	5.22
44	--	5.26
46	--	5.29
48	--	5.34
50	--	5.37
52	--	5.42
54	--	5.43
56	--	5.46
58	--	5.49
60	--	5.50
70	--	5.68
80	--	5.86

La-Sc		
a/o La	DPH	gm/cc
10	69	3.41
25	74	4.03
40	78	4.56
55	79	5.02
70	75	5.66
85	52	5.81

Ce-Y		
a/o Ce	DPH	gm/cc
30	--	5.15
35	--	5.28
40	--	5.36
45	--	5.50
50	--	5.65
55	--	5.73
60	--	5.83
65	--	5.95
70	--	6.07
75	--	6.19

TABLE XVIII (Cont.)

a/o Ce	Ce-Gd DPH	gm/cc
5	41.6	7.83
10	43.0	7.80
15	55.1	7.75
20	66.5	7.72
25	63.4	7.69
27.5	--	7.62
30	53.8	7.62
32.5	--	7.56
35	46.7	7.57
37.5	--	7.39
40	45.8	7.53
45	44.7	7.50

a/o Nd	Nd-Ho DPH	gm/cc
50	73.0	7.79
55	64.5	7.49
60	63.8	7.44
65	47.9	7.22
70	44.3	7.25
71	40.1	7.30
75	44.6	7.07
80	42.6	6.99
85	40.9	6.95
90	--	--

a/o Ce	Ce-Ho DPH	gm/cc
35	60.4	7.81
40	59.8	7.75
45	58.3	7.65
50	58.5	7.56
55	57.3	7.48
60	49.5	7.39
65	51.5	7.28
70	51.9	7.20
75	50.7	7.06

a/o Gd	Gd-Sc DPH	gm/cc
10	55	3.60
25	81	4.48
40	82	5.30
55	79	6.03
70	69	6.67
85	66	7.26

a/o Nd	Nd-Gd DPH	gm/cc
20	65.0	7.70
30	67.0	7.61
35	61.3	7.55
40	50.7	7.49
45	52.0	7.42
50	59.1	7.40
55	53.3	7.35
60	49.4	7.28
65	47.6	7.25
70	44.8	7.21
80	42.0	7.10

a/o Nd	Nd-Y DPH	gm/cc
40	--	5.48
45	--	5.60
50	--	5.72
55	--	5.88
60	--	6.01
65	--	6.14
69	--	6.24
70	--	6.27
75	--	6.41
80	--	6.54
85	--	6.66
90	--	6.77
95	--	6.89

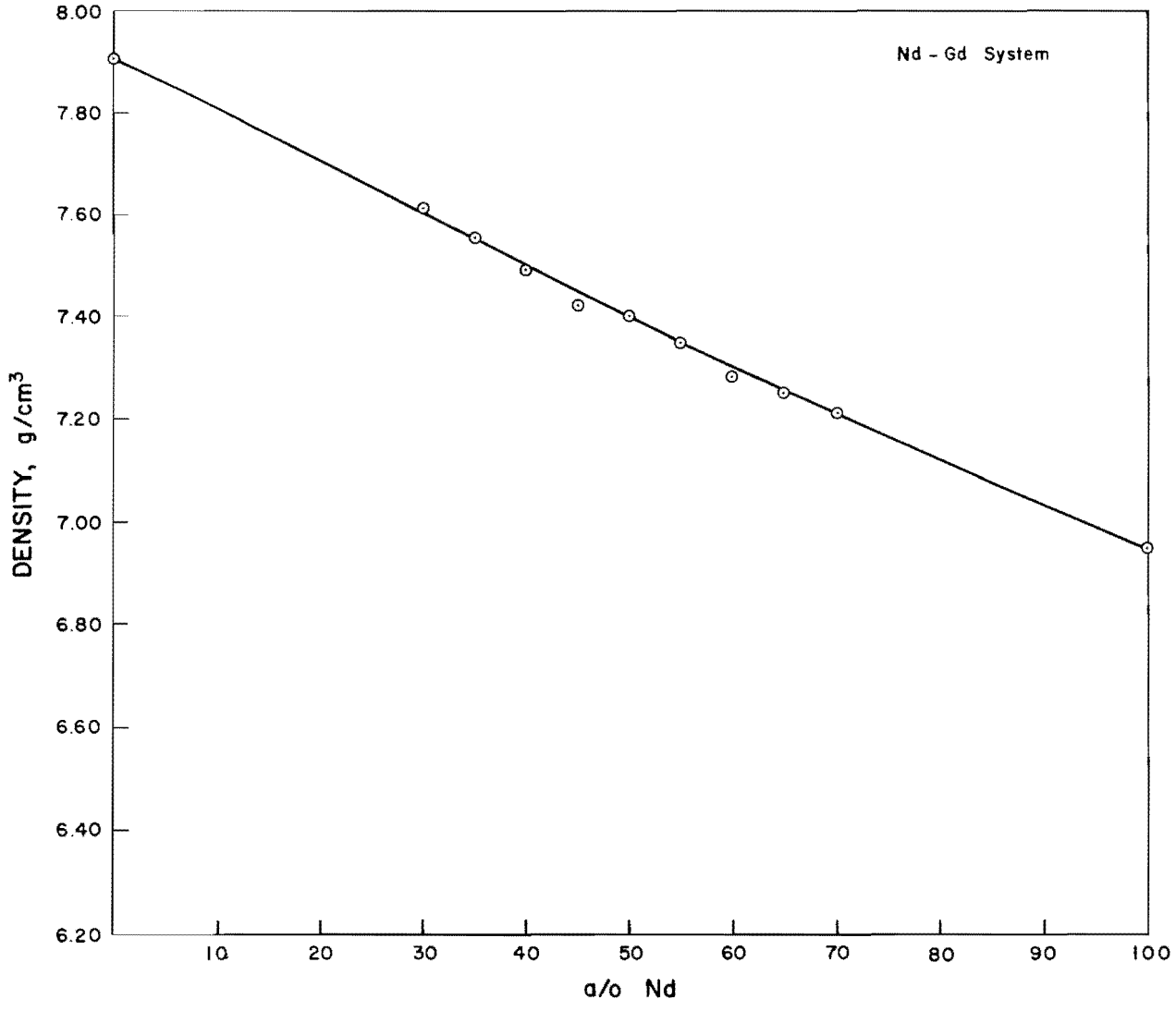

Figure 36. Density Versus Composition for the Nd-Gd System.

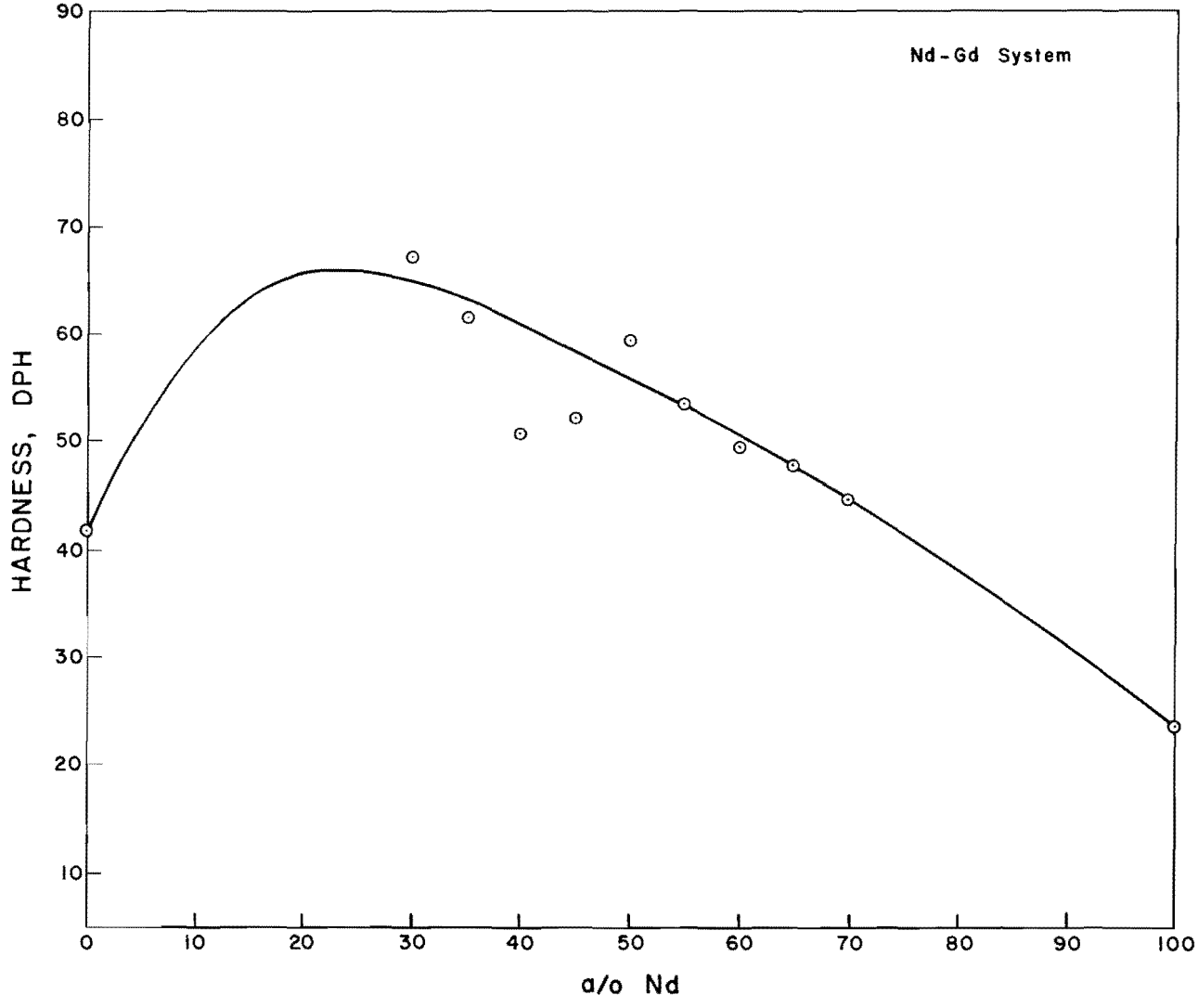

Figure 37. Hardness Versus Composition for the Nd-Gd System (10 Kg, 10X).

The alloys prepared in these systems are presented below.

La-Gd System	Nd-Gd System	Nd-Ho System
a/o La	a/o Nd	a/o Nd
10	10	10
20	20	20
30	30	30
40	40	40
50	50	50
60	60	60
65	70	70
70	80	80
80	90	90
90		
92.5		
95		
97.5		

The thermodynamics of these systems should be very similar to all other intra-rare earth combinations. Specifically, the terminal solid solution and the samarium-type phase regions were analyzed by liquid-metal-solution calorimetry. With this technique the heats of solution of the various pure metals and their alloys in liquid metal were determined. From these data the heat of mixing as a function of composition for each alloy system were determined.

The plot of the heat of mixing versus composition data for any binary system would show abrupt inflections at major phase boundaries if they existed. Thus, experimental thermodynamic data on intra-rare-earth binary systems would be additional verification of the characteristics of the samarium-type structure. Since all of the previous data had negated the presence of a peritectoidally-formed intermediate phase, it was expected to see smooth curves of the thermodynamic data. This was borne out in the actual plots.

A preliminary study was first conducted to determine the ability of liquid tin to dissolve the rare earth metals of interest; La, Nd, Gd, and Ho. Liquid tin has been the traditional metal bath for this equipment. However, after finding that the solution of some of the rare earths, particularly the heavy rare earths, was much too slow to obtain accurate data, it was necessary to adjust several variables. Either the temperature of the bath could be raised or a different bath metal could be developed. The first tin bath was held at 475° C. It was next raised to 500° C, which is the safe upper limit of the calorimeter. The dissolution time decreased, but was still not sufficient. Other baths were tried. Liquid bismuth was attempted next, even though it has a rather high vapor pressure. The dissolution time did not improve. Liquid indium was then employed and the rate of solution was considerably improved. The lanthanum, neodymium, and gadolinium were dissolved very rapidly. The holmium is marginal, but it was believed that good data could still be obtained with holmium. Therefore, it was decided to use liquid indium as the bath throughout the rest of the program.

The calorimeter was calibrated by dropping solid indium samples (~ .4g) between every three unknown rare earth samples. From the known heat content data of indium, the calorimeter heat capacity could be calculated. The values were averaged to determine the calorimeter heat capacity. In order to assure reproducibility and avoid possible intermediate compound formation between indium and the rare earths, only three specimens for each composition were dropped; then, a new indium bath would be installed.

The liquid metal solution calorimeter furnishes a method by which the heat effects accompanying the dissolution of the alloy in the liquid metal of the calorimeter bath are combined with the heat effects of the constituent elements to yield the heats of mixing or formation. Representative equations for these reactions are as follows:

1. $xA(273°K) \rightarrow x\underline{A}\,(750°K)$ ΔH_1
2. $yB(273°K) \rightarrow y\underline{B}\,(750°K)$ ΔH_2
3. $AxBy(273°K) \rightarrow x\underline{A}\,(750°K) + y\underline{B}(750°K)$ ΔH_3

where x and y are mole fractions and $\underline{A}$ and $\underline{B}$ represent the solute dissolved in the liquid metal. Combining equations 1, 2, and 3,

determines the heat of mixing or formation of the alloy or compound from the constituent elements. This heat is given by:

$$\Delta H^{M \text{ or } F}\ (273°K) = x\Delta H_1 + y\Delta H_2 - \Delta H_3$$

The values for the heats of mixing are referred to the initial temperature of the alloy and elements, namely 273°K. The measured heats of solution of the rare earths and alloys in indium are large and negative, and the calculation of the heat of mixing involves differences between large numbers. This increases the error in the calculated heat of mixing.

The measured heats of solution of the pure components and the alloys are tabulated in Table XIX for the three systems studied. The calculated heats of mixing are presented in Table XX. Plots of the heats of mixing versus composition are presented in Figures 38, 39, and 40. The curves are similar in shape, exhibiting a positive heat of mixing in the heavy rare-earth region and a negative deviation in the light-rare-earth region. Thus, the solid solutions throughout each system are definitely not thermodynamically ideal. The deviation from ideality does not show any abrupt inflexions in the curves that could be attributable to the earlier proposed intermediate phase and the immiscibility gaps. However, one can generally say that the heavy-rare-earth region, where the deviation is positive, has a tendency towards like-atom attraction, or an immiscibility gap. Whereas, the regions where the stacking sequences are complex are either becoming more negative (La-Gd system) or are completely negative (Nd-Gd and Nd-Ho systems). This would imply that these two regions have a tendency toward unlike atom attraction, or compound formation. Note, that the La-Gd system shows an anomaly in the graphical plot. The gap in the lanthanum-rich region is due to the fact that these particular alloys would not go into solution, except at a very slow rate. The rate was too slow to obtain accurate heats of solution. The rate of dissolution was gradually slowing down at 40 through 60 a/o La. From 70 to 92.5 a/o the solution was extremely slow. However, abruptly from 95 a/o to pure lanthanum, the solution of the material was normal. The only explanation which can be offered is that a tighter binding in the lattice of these alloys exists. The slow dissolution is not related to the samarium-type structure because it occurs at the other end of the phase diagram. This anomaly was completely reproducible. New alloys and fresh indium baths were tried, and the data were still identical. Thus, this phenomenon is felt to be real.

TABLE XIX

Measured Heats of Solution of Elements and Alloys

La-Gd System

a/o La	Ave. Heat of Solution (cal/g-atom)	No. of Drops
Pure Gd	-47,700	10
10	-48,800	6
20	-49,700	6
30	-50,100	6
40	-48,400	6
50	-45,800	6
60	-43,000	6
65	*	6
70	*	6
80	*	6
90	*	6
92.5	*	6
95	-48,600	6
97.5	-50,000	6
Pure La	-53,400	16

* Dissolved too slowly

Nd-Gd System

a/o Nd	Ave. Heat of Solution (cal/g-atom)	No. of Drops
Pure Gd	-47,700	10
10	-50,500	6
20	-50,200	6
30	-47,600	6
40	-48,200	6
50	-48,900	6
60	-50,000	6
70	-50,200	6
80	-51,400	6
90	-53,400	6
Pure Nd	-54,400	14

TABLE XIX (Cont)

Nd-Ho System

a/o Nd	Ave. Heat of Solution (cal/g-atom)	No. of Drops
Pure Ho	-44,900	2
10	-48,500	3
20	-47,000	3
30	-48,000	6
40	-47,800	6
50	-47,100	6
60	-46,400	6
70	-46,600	6
80	-51,300	6
90	-51,900	6
Pure Nd	-54,400	14

TABLE XX

Heats of Mixing in the Binary Rare-Earth Systems

La-Gd System

a/o La	Heat of Mixing (cal/g-atom)
10	+ 500
20	+ 800
30	+1000
40	-1600
50	-5700
60	-8140
65	*
70	*
80	*
90	*
92.5	*
95	-5500
97.5	-4300

* Dissolved too slowly

Nd-Gd System

a/o Nd	Heat of Mixing (cal/g-atom)
10	+2100
20	+1200
30	-2100
40	-2160
50	-2100
60	-1700
70	-1200
80	-1700
90	- 300

TABLE XX (Cont)

Nd-Ho System

a/o Nd	Heat of Mixing (cal/g-atom)
10	+2700
20	+ 100
30	+ 300
40	-1000
50	-2600
60	-4200
70	-4000
80	-1200
90	-1600

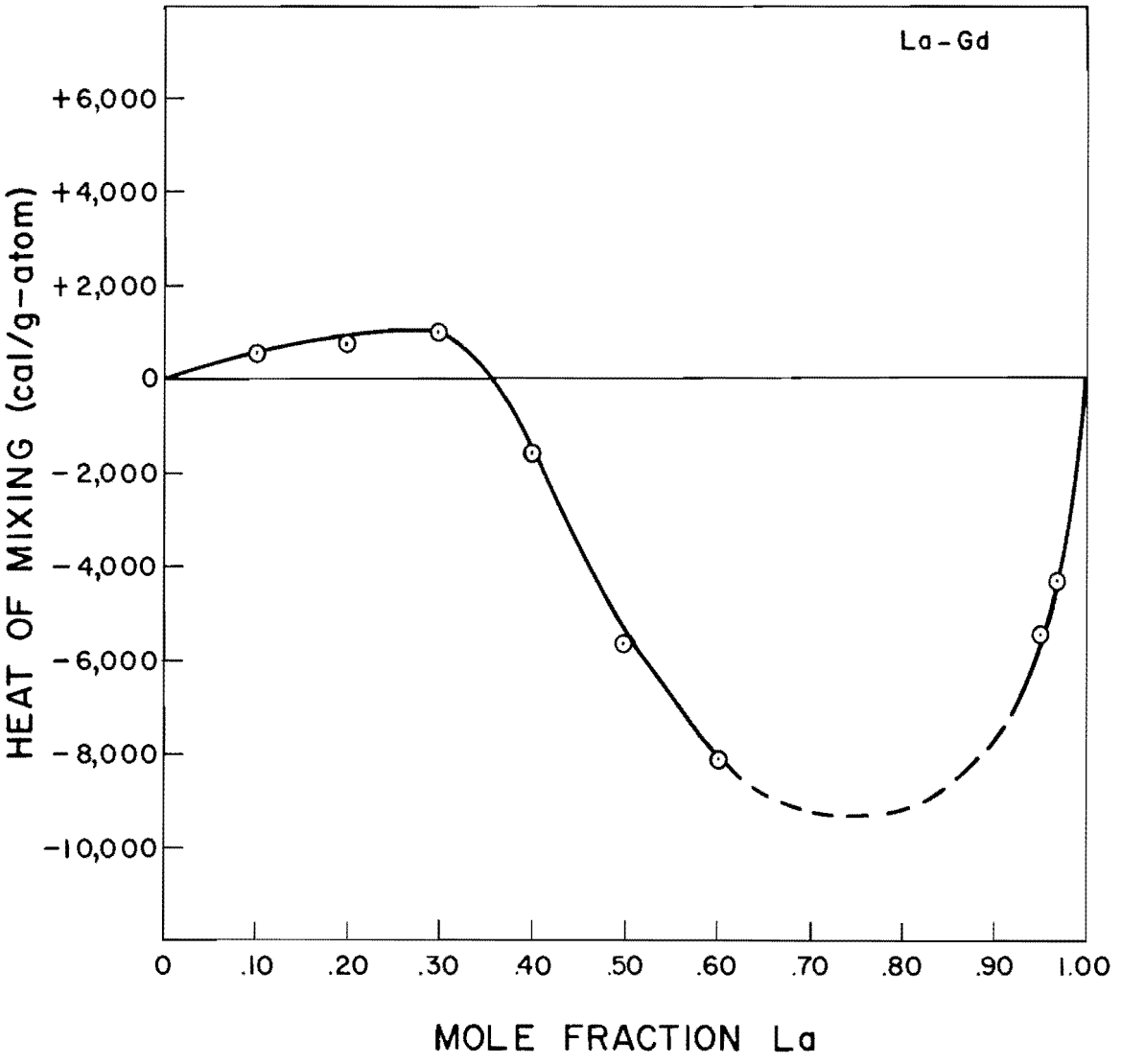

Figure 38. Heat of Mixing at 273K Versus Mole Fraction La for the La-Gd System.

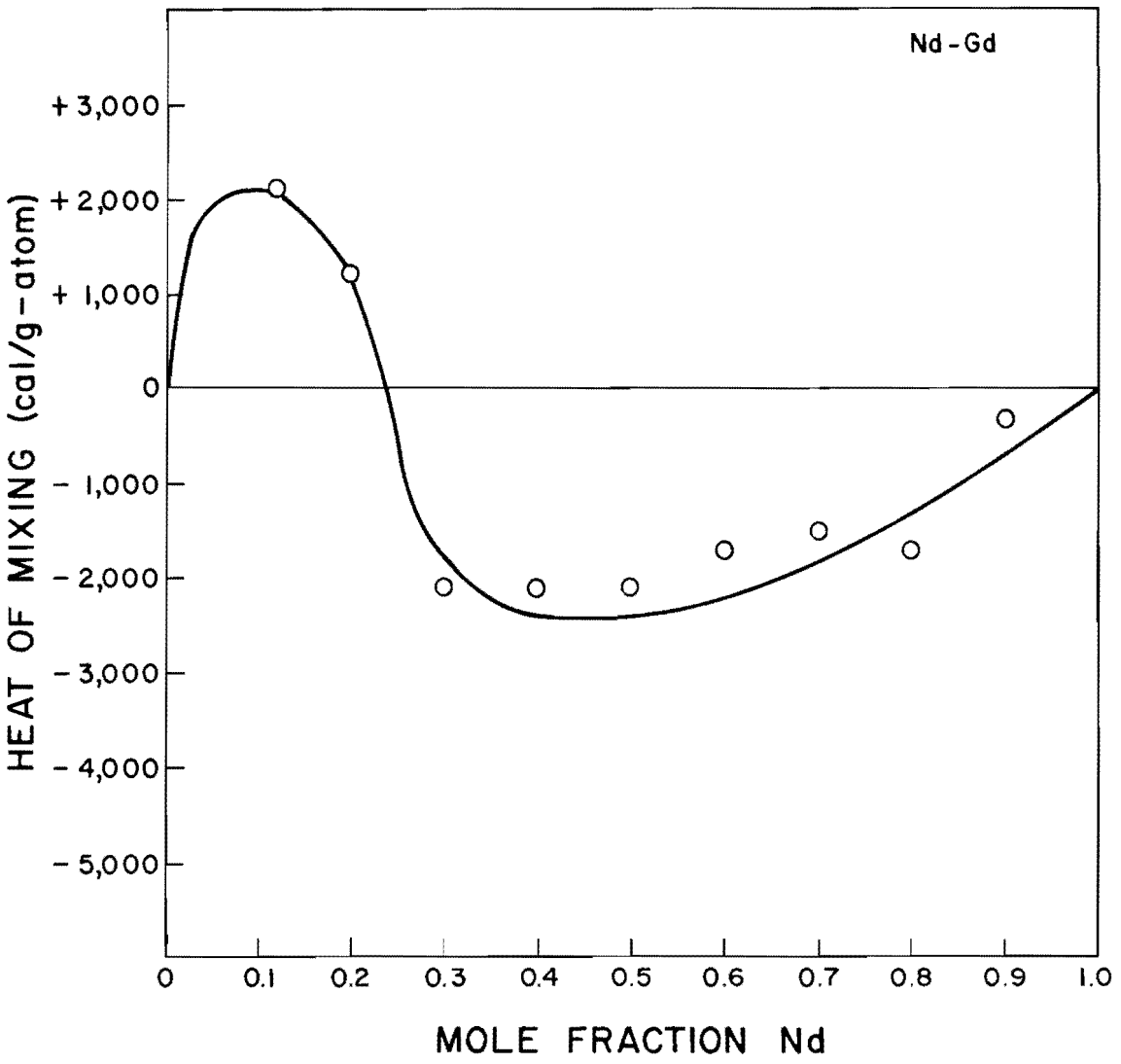

Figure 39. Heat of Mixing at 273K Versus Mole Fraction Nd for the Nd-Gd System.

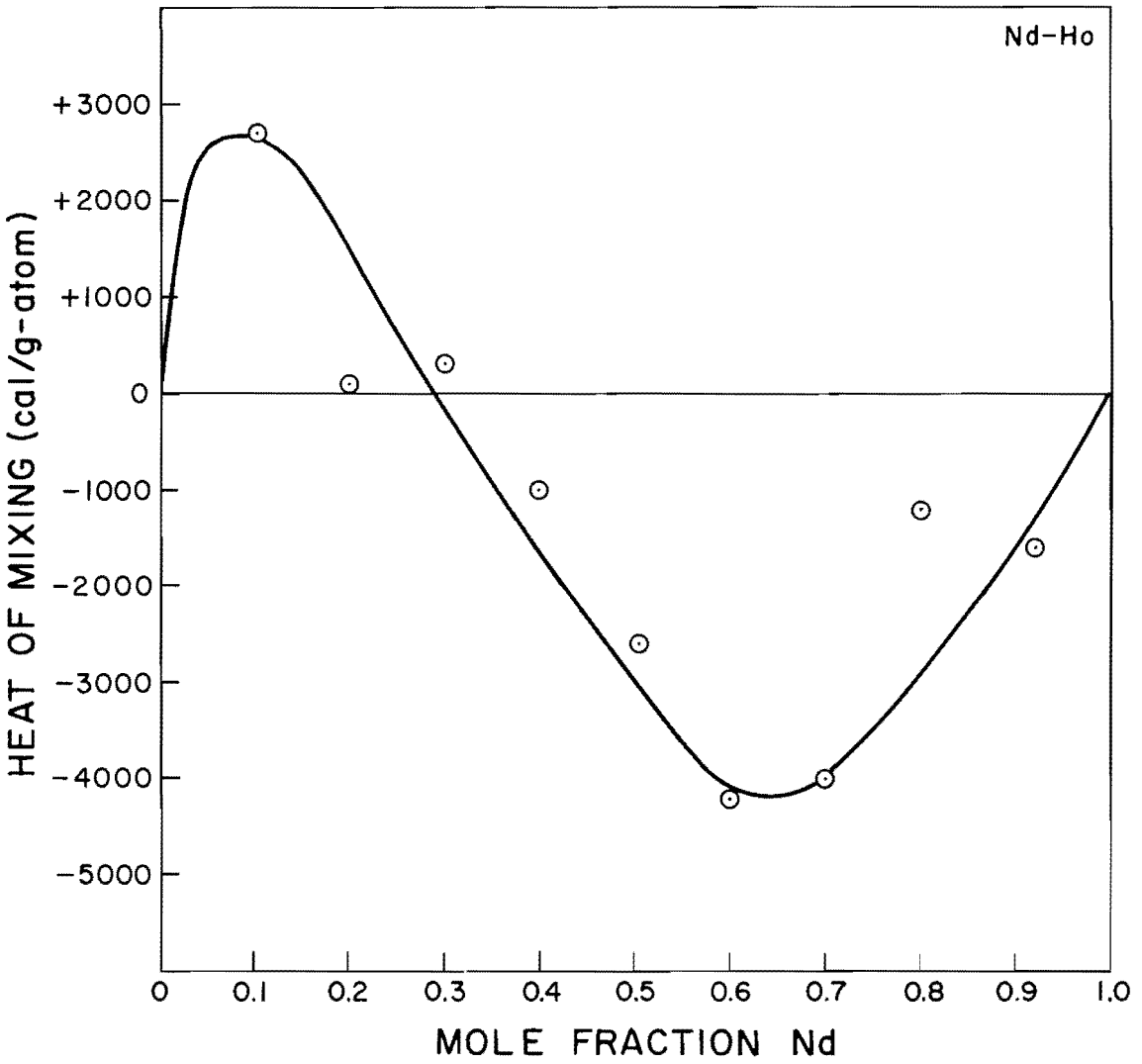

Figure 40. Heat of Mixing at 273K Versus Mole Fraction Nd for the Nd-Ho System.

F. Conclusions

The combined interpretation of the data from the various techniques employed in this study have conclusively proven that an intermediate phase formed by a peritectoid reaction does not exist in binary intra-rare-earth systems consisting of light-and heavy-rare-earth components. As a result the associated phase equilibria first reported are erroneous. Instead, a unique and unparalleled phase exists over a reproducible range of compositions, whose origin is thought to arise from a type of recrystallization which is nucleated and propagated by a microtwinning mechanism. The recrystallized and microtwinned grains have the samarium-type structure. These grains form from the matrix solid solution with no change in composition. The criteria of formation of this phase is that a light-rare-earth be alloyed with a heavy rare earth. The compositional range of existence is analytically predictable. This is determined by employing the lever rule between the atomic number of the components and that of samarium metal. The samarium-type structure appears at the calculated value in the alloy system. This technique is rationalized on the following basis. The reason samarium metal has the samarium-type structure is that it is a transition between the structures of the light rare earths and the heavy rare earths, which is a difference in stacking sequence. A successive electron is added in the 4F shell for each increase in atomic number as one traverses through the elemental rare earth series. The mean atomic radii show an almost linear decrease with atomic number. Thus, in any alloy series between a light and a heavy rare earth, one brackets the whole size range between these two components, but always inclusive of samarium. Thus the samarium-type structure exists in the alloys for the same reason it appears in samarium metal. From these arguments, it is logical to attribute the samarium-type structure either in the element or in light-heavy rare earth binary systems to size effect. This is the correlative factor between the elements and the alloys.

The phase equilibria in the hexagonal-close-packed, low-temperature region of the binary system consists of complete solid solubility throughout the range of compositions. The only inconsistency throughout the solubility range is that of stacking sequence. Three regions of different stacking sequences exist; the light-rare-earth solid solution, the samarium-type structure, and the heavy-rare-earth solid solution. It is within the second range that entirely new grains of the samarium-type phase are formed. The formation of the new grains is felt to be

strain induced. The strain is primarily attributed to size effects, but the grains originate either at the transformation from the body-centered-cubic to the hexagonal-close-packed form or due to thermal fluctuations on cooling from this region. The grains have major orientation differences compared to the matrix out of which they appear, and their boundaries are completely incoherent. The relative amount of this phase increases from either edge of the range of existence until about midpoint where the structure is all samarium-type.

In conclusion, the "synthesis" of a material very similar to samarium metal can be produced by alloying a light rare earth with a heavy rare earth. The "synthesis" is valid both morphologically and structurally.

Acknowledgements

The author wishes to acknowledge the contribution of Mr. Joseph F. Nachman, who was associated with this program during the first half of the program; Messrs George Rauscher and Gavin Mallett for the X-ray diffraction analysis, Mr. Robert McManis and Mrs. Yvonne Shinton who were the principal technicians on the program; Mr. Shou-Shu Shen, the graduate student who did the experimental work on the liquid metal solution calorimeter; and Mr. Arthur Hedin who did the arc melting. Acknowledgement must also be given to Dr. Jerry Rausch and the Office of Naval Research, U. S. Department of the Navy, under whose auspices this work was performed.

IV. REFERENCES

1. C. E. Lundin and D. T. Klodt, APEX Report 424 (August 1958), XDC Report 59-8-187 (Nov. 1958), XDC Report 59-8-188 (Feb. 1959), Contract No. AT-33 with the General Electric Co., ANP Division, Cincinnati, Ohio.

2. F. H. Spedding, R. M. Valletta, and A. H. Daane, ASM Transactions, 1962, Vol. 55, No. 3, p. 483.

3. Howlett, Leach, Ticknor, and Bever, Rev. Sci. Inst., 1962, Vol. 33, p. 619.

4. F. H. Spedding and A. H. Daane, Met. Rev., 1960, Vol. 5, No. 19, p. 619.

5. K. W. Herrman, A. H. Daane, and F. H. Spedding, 1955, Ames Laboratory, Ames, Iowa, ISC-702.

6. K. A. Gschneidner, Rare Earth Alloys, D. Van Nostrand Company, Inc., 1961.

7. C. G. Kirkpatrick and B. Love, Proceedings of the Second Rare Earth Research Conference, Glenwood Springs, Colorado, Gordon and Breach Publishing Co., Sept. 1961.

8. I. V. Burov, V. F. Terechova, and E. M. Savitsky, J. Neorganic Chemistry, 1963, Vol. 12, p. 2685.

9. B. J. Beaudry, M. Michel, A. H. Daane, and F. H. Spedding, Proceedings Fourth Rare Earth Research Conference, Phoenix, Ariz., 1964, to be Published, Sponsored by Arizona State University.

DISTRIBUTION

Recipient	Copy
Chief of Naval Research Department of the Navy Attention: Code 423 Washington, D. C. 20360	3
Commanding Officer Office of Naval Research Branch Office 207 West 24th Street New York, New York 10011	1
Commanding Officer Office of Naval Research Branch Office 495 Summer Street Boston, Massachusetts 02110	1
Commanding Officer Office of Naval Research Branch Office 230 North Michigan Avenue Chicago, Illinois 60601	1
Commanding Officer Office of Naval Research Branch Office 1030 E. Green Street Pasadena, California 91101	1
Commanding Officer Office of Naval Research Branch Office 1000 Geary Street San Francisco, California 94109	1
Assistant Attache for Research Office of Naval Research Branch Office, London FPO New York 09510	5

DISTRIBUTION (Cont.)

Recipient	Copy
Director U. S. Naval Research Laboratory Washington, D. C. 20390 Attention: Technical Information Officer, Code 2000	4
, Code 2020	1
, Code 6200	1
, Code 6300	2
, Code 6100	1
Chief, Bureau of Naval Weapons Department of the Navy Washington, D. C. 20360 Attention: Code RRMA	1
Code RRMA-2	1
Commanding Officer U. S. Naval Air Engineering Center Philadelphia, Pennsylvania 19112 Attention: Aeronautical Materials Laboratory	1
Commanding Officer U. S. Naval Ordnance Laboratory White Oaks, Maryland	1
Commanding Officer U. S. Naval Proving Ground Dahlgren, Virginia Attention: Laboratory Division	1
Chief, Bureau of Ships Department of the Navy Washington, D. C. 20360 Attention: Code 315	1
Code 335	1
Code 341	1
Code 350	1
Code 634	1
Commanding Officer U. S. Naval Engineering Experiment Station Annapolis, Maryland Attention: Naval Alloys Division (Code 860)	1

DISTRIBUTION (Cont.)

Recipient	Copy
Materials Laboratory New York Naval Shipyard Brooklyn, New York 11201 Attention: Code 907	1
Commanding Officer David Taylor Model Basin Washington, D. C.	1
U. S. Naval Postgraduate School Monterey, California Attention: Department of Chemistry & Material Science	1
Commanding Officer U. S. Naval Ordnance Test Station China Lake, California	1
Defense Documentation Center Cameron Station Alexandria, Virginia 22314	20
Commanding Officer Army Materials Research Agency (AMRA) Watertown Arsenal Watertown, Massachusetts	
Attention: Research Programs Office (AMXMR-P)	1
Technical Library (AMXMR-ATL)	1
Commanding Officer Army Research Office, Durham Box CM, Duke Station Duke University Durham, North Carolina Attention: Metallurgy Division	1
U. S. Air Force ARDC Office of Scientific Research Washington, D. C. 20333 Attention: Solid State Division (SRQB)	1
National Bureau of Standards Washington, D. C. 20234	
Attention: Metallurgy Division	1
Inorganic Material Division	1

DISTRIBUTION (Cont.)

Recipient	Copy
U. S. Atomic Energy Commission Washington, D. C. Attention: Technical Library	1
Metals and Materials Branch	1
Argonne National Laboratory P. O. Box 299 Lemont, Illinois	1
Brookhaven National Laboratory Technical Information Division Upton, Long Island New York Attention: Research Library	1 1
Union Carbide Nuclear Company Oak Ridge National Laboratory P. O. Box P Oak Ridge, Tennessee Attention: Metallurgy Division	 1
Solid State Physics Division	1
Los Alamos Scientific Laboratory P. O. Box 1663 Los Alamos, New Mexico Attention: Report Librarian	1
U. S. Atomic Energy Commission New York Operations Office 70 Columbus Avenue New York, New York Attention: Document Custodian	1
University of California Radiation Laboratory Information Division Room 128, Building 50 Berkeley, California	1
Commanding Officer U. S. Naval Ordnance Underwater Station Newport, Rhode Island	1

DISTRIBUTION (Cont.)

Recipient	Copy
Aerospace Research Laboratories (ARZ) Building 450 Wright-Patterson AFB, Ohio 45433	1
Defense Metals Information Center Battelle Memorial Institute 505 King Avenue Columbus, Ohio 43201	2
Solid State Devices Branch Evans Signal Laboratory U. S. Army Signal Engineering Laboratories c/o Senior Navy Liaison Officer U. S. Navy Electronic Office Fort Monmouth, New Jersey	1
Commanding General U. S. Army, Frankford Arsenal Philadelphia, Pennsylvania 19137 Attention: Mr. Harold Markus ORDBA-1320, 64-4	1
Executive Director Materials Advisory Board NAS-NRC 2101 Constitution Avenue Washington, D. C. 20418	1
Dr. G. S. Ansell Associate Professor of Metallurgical Engineering Rensselaer Polytechnic Institute Troy, New York 12181	1
Professor H. Brooks Dean of Graduate School of Applied Science Harvard University Cambridge, Massachusetts	1
Professor C. L. Corey Department of Chemical & Metallurgical Engineering Wayne State University Detroit, Michigan	1

DISTRIBUTION (Cont.)

Recipient	Copy
Professor J. J. Duga Battelle Memorial Institute 505 King Avenue Columbus, Ohio 43201	1
Professors P. Gordon and D. Rausch Metallurgical Engineering Department Illinois Institute of Technology Chicago, Illinois 60616	1
Professor N. J. Grant Department of Metallurgy Massachusetts Institute of Technology Cambridge, Massachusetts 02100	1
Drs. D. Hamilton and B. Shaw Research and Development Center Westinghouse Electric Corporation Pittsburgh, Pennsylvania 15213	1
Dr. R. I. Jaffee, Associate Manager Department of Metallurgy Battelle Memorial Institute 505 King Avenue Columbus, Ohio 43201	1
Dr. L. Kaufman Director of Research Manufacturing Laboratories, Inc. 21 Erie Street Cambridge, Massachusetts 02100	1
Dr. Alan Lawley Physics of Metals Laboratory Franklin Institute Philadelphia, Pennsylvania 19104	1
Dr. Charles E. Lundin Physical Metallurgy Department Denver Research Institute Denver, Colorado 80210	1

DISTRIBUTION (Cont.)

Recipient	Copy
Professor F. Seitz National Academy of Sciences 2101 Constitution Avenue, NW Washington, D. C.	1
Dr. M. Semchyshen Director, Metallurgical Research Climax Molybdenum Company Detroit, Michigan	1
Professors B. Taggart and D. Polonis School of Mineral Engineering University of Washington Seattle, Washington 98105	1
Professor Johannes Weertman Department of Material Sciences Northwestern University Evanston, Illinois	1
Professor R. Roy Materials Research Laboratory 1-112 Research Building Pennsylvania State University University Park, Pennsylvania 16802	1